JOURNAL OF GEOPHYSICAL RESEARCH, VOL. 106, NO. A11, PAGES 26,243–26,260, NOVEMBER 1, 2001

# The Io mass-loading disk: Model calculations

Yongli Wang, Christopher T. Russell, and Joachim Raeder

Institute of Geophysics and Planetary Physics, University of California, Los Angeles

**Abstract.** The observations of ion cyclotron waves up to 0.5 $R_J$ beyond the orbit of Io are best explained by the presence of a thin disk of fast neutrals whose ionization and pickup provide the free energy for the waves. We extend the model of *Wilson and Schneider* [1999] in order to explain the observed properties of this mass-loading region, especially the most recent Galileo observations near Io. In the extended model, some of the molecules of sulfur compounds in Io's exobase are first ionized by photoionization, impact ionization, and charge exchange. These charged particles are accelerated in the corotation electric field associated with the motion of the magnetized Io torus plasma that is moving through its exosphere. After a period of acceleration the heavy ions are neutralized by charge exchange with other exospheric neutral particles or combined with local electrons. These newly neutralized particles continue with high velocities similar to those of their former charged state, moving only under the influence of the gravity fields of Jupiter and Io, not affected by the electric and magnetic field. If they do not impact Io or its atmosphere, these neutral particles can propagate large distances across the magnetic field before they are reionized. Eventually, the reionized particles are lost by dissociation. Characteristic Io mass-loading particle distributions, such as high torus plasma density outside Io's orbit and the lower density inside, and the directional feature of the mass-loading neutral cloud, are qualitatively reproduced in the model. Meanwhile, the configuration of the mass-loading region, in which the ion cyclotron waves are observed, is obtained, and the results are consistent with Galileo wave observations. Three parameters are found to control the structure of the neutral and ion loading disks: the characteristic lifetimes of the initially created ions, of the neutral molecules, and of the ions generated by neutral particle reionization. In addition, particle source geometry, gravity, and the near Io field configurations play important roles in the Io mass-loading process.

## 1. Introduction

The atmosphere of Io supplies the Jovian magnetosphere with as much as several tons of mass per second [*Dessler*, 1980; *Brown*, 1994]. Io orbits near the magnetic equatorial plane of Jupiter in a strong magnetic field (~2000 nT). This strong magnetic field couples the Io torus to the rapidly rotating Jovian ionosphere, and the newly created ions are accelerated to up to twice the corotation velocity. Io interacts with the torus plasma much like a comet interacts with the solar wind, but in a significantly stronger magnetic field. This interaction is very complex, and many processes, for example, the interaction between Io's atmosphere and the corotating magnetospheric plasma and photochemical processes, can affect the escape of iogenic particles. It is the purpose of this paper to develop a simple model that contains the essential elements of the mass-loading process, that explains the observations of ion cyclotron waves at Io, and that is consistent with observations of the torus.

Ground observations over the past decades have shown the structure of the ejected particles around Io [*Matson et al.*, 1978; *Pilcher et al.*, 1984]. Spacecraft observations of the Jovian magnetospheric plasma began with Pioneer 10 and 11 [*Intriligator and Miller*, 1981] and were followed by Voyager 1 and 2 Jupiter flybys on March 5 and July 9, 1979, respectively [*Bagenal et al.*, 1980]. The Voyager 1 in situ plasma measurements through the Io torus brought new understanding to Io and its torus, including in situ torus density and temperature, and torus plasma waves [*Bridge et al.*, 1979; *Goldberg et al.*, 1980; *Kumar*, 1984; *Thorne and Scarf*, 1984; *Bagenal*, 1985]. Galileo, in orbit around Jupiter, has provided an unprecedented opportunity to study the Io plasma torus. Especially the Io flybys on December 7, 1995 (I0), October 11, 1999 (I24), November 26, 1999 (I25), and February 22, 2000 (I27), provided new data sets of the field structure, wave properties, and the Io-torus interaction near Io [*Kivelson et al.*, 1996; *Huddleston et al.*, 1999; *Russell et al.*, 1999; *Russell and Kivelson*, 2001]. However, they also have revealed the complexity of the Io mass-loading process [*Russell et al.*, this issue].

A surprise of the initial Galileo data was the size of the mass-loading region. Ion cyclotron waves were seen out to more than 15 $R_{Io}$(0.4 $R_J$) from Io [*Kivelson et al.*, 1996] even though they were absent on Voyager 1's pass 10 $R_{Io}$ below Io. This observation is particularly important because in the region close to Io there is only about 200 kg $s^{-1}$ added to the torus, not a ton $s^{-1}$ [*Bagenal*, 1997]. A wide dispersal of the neutrals away from the immediate vicinity of Io would help resolve this discrepancy, but we need to understand how this wide dispersal is accomplished. The neutral cloud released by Io cannot be isotropic because Voyager 1 did not detect ion producing waves 10 $R_{Io}$ beneath the moon. A disk-



Paper number 2001JA900062.
0148-0227/01/2001JA900062$09.00

shaped geometry in which the neutral cloud stayed near the plane defined by the location of Io and the flow direction and the electric field would be consistent with both the Voyager and Galileo data.

Many models have been proposed to explain the mass-loading process and its observational characteristics, such as the model by *Pilcher et al.* [1984]. In their study, a directional feature, which was directed away from Jupiter and oscillated north and south of Io's orbital plane, was obtained from sodium $D_2$-line intensity observations. The directional feature was attributed to a magnetospheric-wind-driven gas mechanism with the possible involvement of sputtering of the near right-angle source by particle scattering. A new Io mass-loading model [*Wilson and Schneider*, 1999], hereinafter called the WS model, was recently proposed to explain the directional feature. In this model, particles are first ionized in Io's ionosphere. Then they are accelerated to a speed as high as about twice the plasma corotation speed, after which they are neutralized through charge exchange. Since neutral particles are not subject to electromagnetic forces, they propagate outward in the gravity fields of Jupiter and Io and can reach large distances from Io. Some of these neutrals may then become ionized again at large distances from Io. The large-scale structure of the WS model has been calculated and is consistent with ground observations, though no small-scale structure results are given. A restricted source region is used in the Wilson and Schneider model calculations, unlike the source region in our model.

In this paper we study step by step the effects of different factors on Io mass loading, such as the shape of the source, gravity, and the reionization process. Small-scale characteristics of Io mass loading are addressed. Finally, we extend the WS model, giving more consideration to the initial particle distribution in phase space and the reionization of neutral particles that is followed by dissociation. Statistical neutralization, ionization, and dissociation rates are used to simulate these processes in the mass loading. Steady spatial loading patterns for neutrals and ions are obtained, and their characteristics, including the density distribution and possible temperature implications, are obtained. Three major parameters, the characteristic lifetimes for the initial ions, the neutral particles, and the final ions, are identified as contributing most to the structure of the Io mass-loading disk. Finally, the advantages and disadvantages of this model are discussed and possible ways to improve the model are proposed.

## 2. Observations

### 2.1. Imaging and Spectroscopic Observations

Io's atmosphere is dominated by $SO_2$ and its dissociation products SO, O, and S. $SO_2$ is released from the volcanos on Io and is found in deposits on the surface. Galileo imaging has shown that blue glows, which are possibly due to electron impact on molecular $SO_2$, emanate from at least five volcanic plumes near Io's equator [*Geissler et al.*, 1999]. Thus the $SO_2$ is released from Io and its atmosphere can be expected to be highly variable in time and space. Io's atmosphere has been probed at wavelengths in the infrared, millimeter, and ultraviolet [*Pilcher et al.*, 1984; *Lellouch et al.*, 1990, 1992; *Lellouch*, 1996; *Ballester et al.*, 1994; *Hendrix et al.*, 1999]. However, many detailed properties of Io's atmosphere, such as its density, composition, thickness, and time variability, are still uncertain [*Lellouch*, 1996].

Because of its large cross section for resonant scattering of sunlight, sodium has often been used by ground imaging and spectroscopic observations, though it is only a trace constituent of Io's atmosphere [*Brown*, 1994]. For most atmospheric escape processes, sodium is considered a good tracer of the more abundant atmosphere species, such as $SO_2$ [*Ballester et al.*, 1994]. Thus the general spatial distribution of sodium should reflect the spatial distribution of sulfur and its compounds, but direct correlation can only be used with caution because of the differences between sodium and sulfur compounds, for example, their different photochemical characteristics. One of the most prominent features of the Io plasma torus is the so-called directional feature. From early ground optical and spectral observations [*Matson et al.*, 1978; *Pilcher et al.*, 1984], and later confirmed by in situ satellite observations [*Burger et al.*, 1999], it was found that there is a neutral structure that extends almost radially outward from Io. This structure is very sharp and bounded by strong gradients, which makes it unlikely that it can be formed solely by diffusive processes. By studying Galileo's close-up images of the Io sodium jet, *Burger et al.* [1999] also found that Io's directional feature is mainly concentrated at low latitudes. Lyman $\alpha$ imaging of the $SO_2$ distribution on Io similarly showed a higher $SO_2$ density concentration near the equator than at Io's poles [*Feldman et al.*, 2000].

### 2.2. Background Magnetic Field

The magnetic field at Io is close to 2000 nT, varying slightly with the Jovian magnetic latitude of Io at the encounters. The field increases on the upstream side and decreases on the downstream side to form a wake region. Large magnetic field variations are confined to about 1 $R_{Io}$ above the surface of Io [*Kivelson et al.*, 1996]. Farther away from Io the magnetic field changes slightly over large distances compared with Io radius.

### 2.3. Magnetic Field Oscillation Observations

Galileo magnetic field oscillation observations near Io provide very important information about the Io's mass-loading process, which greatly compensate the conventional methods in this study. For example, wave observations can provide information about the loading regions of $SO_2^+$ and $SO^+$. Further study of these waves can provide knowledge about the density distribution in this region. Sudden ion cyclotron wave power jumps between upstream and downstream of the torus near Io observed during I24 and I27 Galileo Io flybys support a possibly new loading structure of $SO_2^+$ and $SO^+$, which is different from the well-known banana-shaped loading pattern for sodium [e.g., *Smyth and Combi*, 1988]. Detailed discussion and implications of the wave observations of the several Galileo Io flybys are given by *Russell et al.* [this issue]. Dispersion analysis of the plasma wave observations is performed by *Blanco-Cano et al.* [this issue].

### 2.4. Plasma Observations

The torus plasma properties can be inferred from the imaging and spectrum observations discussed above, but the results are subject to certain ambiguities. In situ plasma observations provide more direct knowledge of the torus plasma environment. *Bagenal et al.* [1980] analyzed Voyager 1 in situ measurements of ion densities and temperatures and produced profiles of these plasma parameters along the spacecraft inbound trajectory. A model of the Io plasma torus based on Voyager 1 in situ plasma observation results was constructed [*Bagenal and Sullivan*, 1981]. Direct observations of plasma densities, ion composition, plasma temperature, and flow velocities were made by the Galileo plasma analyzer (PLS) [*Frank et al.*, 1996] and provide an important observation basis for many subsequent model studies near Io [e.g., *Linker et al.*, 1998]. Measurements of electron density

made by the plasma wave subsystem instruments on Galileo during its pass through the torus on December 7, 1995, were analyzed by *Bagenal et al.* [1997]. Both consistencies and inconsistencies were found with Voyager 1 measurements in this study. From the study of the angular distribution of the ions measured by the Galileo plasma spectrometer on the J0 pass leading to the Io flyby, *Crary et al.* [1998] determined the composition and temperature of Io plasma torus. Similar to the results of the inner torus by *Bagenal* [1985], the plasma was found to be dominated by $O^+$. Unlike the Voyager results, however, the ion temperature was found not to be in thermal equilibrium in this study. More recently, *Russell et al.* [2000] have used depleted magnetic flux tubes to probe the ion temperature and confirmed with contemporaneous measurements the rather cool ion temperature obtained by *Crary et al.* [1998] in the torus, but this study also showed that the temperature in the torus was variable.

# 3. Model Description

## 3.1. Overview

Before we describe our model, it is important to have an overview of the chemical reactions that occur in the Io mass-loading process. The chemistry associated with the exosphere of Io and its interaction with the Jovian magnetosphere is very complex, as has been discussed in many studies [e.g., *Summers and Strobel*, 1996; *Smyth and Marconi*, 1998; *Wong and Smyth*, 2000]. Many reactions, such as photoionization, charge exchange, and impact dissociation, are involved in this process.

The principal source components of the mass-loading particles are $SO_2$ and SO, the dominant constituents of the Io atmosphere. The ultimate products of mass loading are $O^+$, $O^{++}$, $S^+$, $S^{++}$, and $S^{+++}$, the major components in the Io torus. Many transitions may be experienced before a neutral particle is mass loaded, and multiple ions, instead of one, may result. The existence of dissociation, recombination, and reneutralization among different species of particles (e.g., $SO_2$, SO, S, O, Na, $H_2S$, $SO_2^+$, $SO^+$, $S^+$, $O^+$, and $Na^+$) greatly complicates this process. A convenient simplification of the mass-loading process is to assume that there is only one characteristic heavy particle species involved in this process. Dissociation, recombination, and charge exchange with particles other than electron will be ignored herein. Ionization and reneutralization will be simplified, and the only other components involved are electron and sunlight. Now there are basically two types of loading process. Using A to denote the characteristic particle, we can schematically illustrate these as

Type 1 $\quad A \rightarrow A^+$

Type 2 $\quad A \rightarrow A^+ \rightarrow A \rightarrow A^+.$

The ionization and reneutralization steps in the second type of mass loading can be repeated. Far away from Io, we can neglect this case because of the largely reduced rate of reneutralization. Type 1 is the scheme commonly used in Io mass loading studies, including the sputtering model. Type 2 is different from type 1 by the presence of a neutralization step. This can produce much higher neutral particle velocities (as high as 114 km $s^{-1}$ relative to Io) compared with common sputtering model velocity (usually $\leq$10 km $s^{-1}$ and $\sim$3 km $s^{-1}$ in many cases) [*Smyth and Combi*, 1988], which can propagate across magnetic field much more easily.

A practical application of the type 2 process is SO mass loading. The type 1 SO loading process, because of the low velocity of the neutral molecule, takes a long time to form a large spatial structure. For a neutral particle speed of 5 km $s^{-1}$, it takes 4 hours to reach 40 $R_{Io}$ from Io ($\sim$1 $R_J$), which is larger than the most efficient SO dissociation, electron impact dissociation, lifetime of around 2 hours near Io. During this time many other reactions happen. In a type 2 process the large speed will ensure fewer other reactions take place other than the common ionization and neutralization of $SO_2$. For neutral particle speed of 40 km $s^{-1}$, it takes only 0.5 hours to reach 40 $R_{Io}$ from Io, which is smaller than electron impact dissociation lifetime. Because of the existence of $SO_2$ dissociation, a comparable number of new $SO^+$ ions originate from $SO_2$ [*Smyth and Marconi*, 1998]. Thus we have to be cautious when we analyze the model density distribution results, but this does not affect the spatial geometry of the mass-loading particles. Further, since SO may have a much more uniform distribution around the Io equator than $SO_2$ [*Wong and Smyth*, 2000], it is easier for us to study the geographical effects of the source while at the same time producing results that can be used for qualitative comparison with observations.

A major difficulty of this scenario is the existence of relatively rapid dissociation of SO and $SO^+$. Since most of SO and $SO^+$ are dissociated, how can we use a multistep model to describe SO loading? This can be overcome by the fact that in order to study the SO and $SO^+$ spatial loading patterns and make comparison with wave observations, we need only investigate the distribution of SO and $SO^+$. The dissociation products of SO and $SO^+$ do not matter much. Though recombination can produce SO and $SO^+$, this occurs much more slower than the dissociation of SO and $SO^+$. Knowing this, we can further study the influence of the dissociation on the lifetimes of SO and $SO^+$. Let us take SO ionization as an example. We assume constant reaction rates for dissociation and ionization and use $\tau_{dis}$ to denote dissociation lifetime and $\tau_{ion}$ to denote ionization lifetime. We also assume that dissociation and ionization are the only reactions for SO. The equation for the evolution of SO density is

$$\frac{dn}{dt} = -n\left(\frac{1}{\tau_{dis}} + \frac{1}{\tau_{ion}}\right), \tag{1}$$

from which we can get the density of SO at time $t$:

$$n = n_0 e^{-t\left(\frac{1}{\tau_{dis}} + \frac{1}{\tau_{ion}}\right)}. \tag{2}$$

In the case of $\tau_{dis} \ll \tau_{ion}$, we have

$$n \simeq n_0 e^{-\frac{t}{\tau_{dis}}}, \tag{3}$$

which means the effective lifetime of SO is $\tau_{dis}$ instead of $\tau_{ion}$. Similar calculations can be done for $SO^+$. Processes other than dissociation that contribute to the depletion of SO and $SO^+$ can be treated in the same way. Though dissociation plays a major role in the different loading phases of SO, different lifetimes should be chosen, as will be discussed in section 3.3, because of the different chemical processes and background environments.

In a later part of the study we construct a type 2 loading model to describe SO mass loading, which can be compared directly with recent Galileo $SO^+$ wave observations. A more detailed discussion about Io's atmospheric and ionospheric chemical reactions is given by *Summers and Strobel* [1996]. $SO_2$ chemical reactions in mass loading are summarized by *Smyth and Marconi* [1998]. We assume SO has an electron impact dissociation lifetime similar to $SO_2$, which is reasonable from the similar wave power profile from wave observations [*Russell et al.*, this issue].

## 3.2. The Model

Complexities arising from different loading steps under various environmental influences (i.e., source geometry and electric, magnetic, and gravity fields) make it difficult to

study Io mass loading from a purely analytical approach. Thus we use Monte Carlo particle simulation as the basic tool in this study. In the following sections we outline the major components of the model that we used in this study.

The basic mechanism of the Io mass-loading process considered in our model is shown in Figure 1. The model has three major steps. The first step is the ionization of Io's atmosphere neutral particles and their acceleration in the corotation electric field. Ionization can be caused by impact ionization by torus electrons, charge exchange between Io's neutrals and the torus ions, and photoionization. The second step is the neutralization of the newly charged particles and the propagation of the neutral particles in the gravity fields of Io and Jupiter. This can occur by charge exchange between the new ions and atmospheric neutral particles and by electron-ion neutralization. The third step is the reionization of the neutral particles generated in the second stage, corotating of the ions with torus plasma, and their final dissociation. A more detailed description of these processes is listed below.

**3.2.1. Particle ionization in Io's atmosphere.** Several processes contribute to the ionization of SO at Io's exobase. Electron impact ionization may be most important. The $SO_2$ ionization lifetime is around 20 hours near Io [*Smyth and Marconi*, 1998]. A similar SO ionization lifetime appears to exist based on the similar radial variation of wave power on the several Galileo Io flyby observations [*Russell et al.*, this issue] albeit with some variation with the solar phase angle of Io in its orbit. Because of the highly variable torus electron density, the electron impact ionization rate can be much different. Especially when we are far away from Io torus, the electron density is much lower and this lifetime can be orders larger than 20 hours. Another way to ionize SO is by photoionization. SO photochemistry is driven by absorption of solar UV radiation. The photon flux has a strong solar zenith angle dependence. In the subsolar atmosphere the ionization rate by photoionization is largest, and it decreases toward zero at the Io optical umbra. Thus the photoionization process depends on the local time. The lifetime of SO by photoionization near the Io exobase is several orders larger than that of electron impact ionization. Charge exchange with torus ions, such as $O^+$ and $S^+$, can also ionize SO. Near Io the SO lifetime by this mechanism is usually larger than that by the electron impact ionization. Similar to electron impact ionization, it is also strongly variable with location.

Once new $SO^+$ ions are created, they are accelerated by the corotation electric field and begin to gyrate. Because the velocity of Io with respect to Jupiter's magnetosphere is ~57 km $s^{-1}$, the ions can reach velocities of up to ~114 km $s^{-1}$

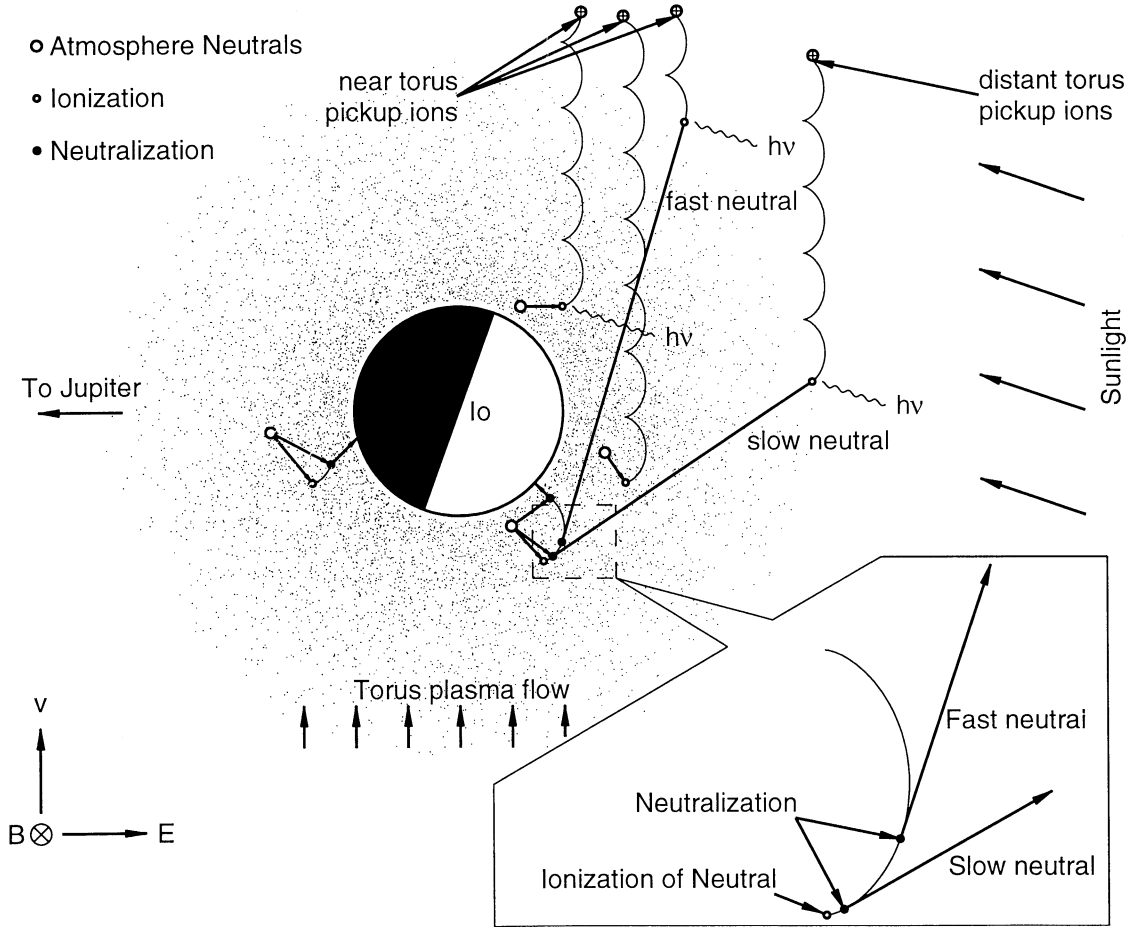


**Figure 1.** The basic mechanism of Io mass-loading process considered in the model. Three basic processes in the model are shown: ionization of neutral atmosphere particles, neutralization of newly born charged particles, and reionization of the neutral particles after they travel some distance away from Io. New ions on the left side of Io are lost in the atmosphere because of the field configuration. Ions coming from reionization will be lost by dissociation, and this is not shown in the figure.

relative to Io. In our model a simple stationary corotation electric field, $\mathbf{E} = -\mathbf{V} \times \mathbf{B}$, is adopted, where $\mathbf{B}$ is Jupiter's dipole magnetic field and $\mathbf{V}$ is the torus plasma corotation velocity.

**3.2.2. Particle neutralization.** $SO^+$ neutralization can occur by charge exchange between $SO^+$ and the neutral particles of Io's atmosphere. Charge exchange with SO and sodium can produce $SO^+$ with a lifetime of about 30 hours near Io exobase, and this value usually increases farther away from Io because of the lower density of SO and sodium. Much quicker dissociation of $SO^+$ can be caused by electron impact dissociation, with a lifetime of the order of hours. Recombination of $SO^+$ with electrons is another way to produce neutral SO, with a possible lifetime of $SO^+$ much longer than 2 hours. A characteristic lifetime of the ions before they are ionized, $\tau_{SO^+,1}$, can be used to denote how long it usually takes before an $SO^+$ is neutralized. In our model calculation we assume no velocity change during $SO^+$ neutralization, though charge exchange can change it in reality.

Neutralization is more likely to occur low enough in the exobase that there are sufficient neutral particles for charge exchange and electrons for recombination but high enough that the ions will experience the torus electric field and the resulting neutral particles with high velocity will survive collision loss and escape. After neutralization, SO neutrals move only in the gravity fields of Io and Jupiter and thus can be transported more easily across the magnetic field to large distances.

**3.2.3. Particle reionization.** Eventually, the neutrals produced in the previous step will be ionized. The three mechanisms discussed in section 3.2.1 contribute to this process. Since the ionization usually happens after neutral particles have moved across the magnetic field with a large speed for some hours, a large spatial distribution of neutrals forms. In this case, electron impact ionization and charge exchange can be much slower than the initial ionization, while the photoionization rate stays almost unchanged.

A characteristic time for the neutral particles to travel across the magnetic field before they are ionized, $\tau_{SO}$, can be used to denote how long neutral particles can survive. After reionization, the new ions will drift in Jupiter's magnetic field and corotation electric field along a circular trajectory around Jupiter until finally dissociated. No neutralization will be considered in this case because of the much lower neutralization rate far away from Io. We use $\tau_{SO^+,2}$ to denote how long the final $SO^+$ ions usually live before they are dissociated.

## 3.3. Numerical Model Description

Near the orbit of Io the gravitational acceleration of Jupiter is about 0.7 m $s^{-2}$. Io's surface gravitational acceleration is about 1.8 m $s^{-2}$ and equals that of Jupiter at a distance of ~1.6 $R_{Io}$ from Io. Thus, at lower altitudes, Io's gravity dominates. In the WS model, Io's gravity is not considered in calculating particle motion. This treatment works well if the particle velocity at the beginning is large, which is the case in the WS model, because particles can propagate a long distance from Io in a short time, where the gravity of Io becomes much smaller than that of Jupiter. Since we are treating new ions in a distributed phase space at the Io surface by giving them different lifetimes for acceleration, there are a certain number of slow particles. We expect that their motion will be controlled more by Io gravity than Jupiter gravity at the beginning of the loading process, which can affect their final spatial distribution.

If ionization occurs deep in the atmosphere of Io, the ion will most likely stay below the exobase of atmosphere because of the frequent collisions. We also expect any plasma drift velocity in the collisional region to be small. At altitudes much higher than the exobase, the particle density is low and the rate of ionization and the contribution to mass loading from this region is small. To simplify our boundary conditions, we use the exobase of Io's atmosphere as the source of newly ionized particles, as was done in many of the former studies [e.g., *Smyth and Marconi*, 1998; *Wilson and Schneider*, 1999]. Various exobase altitudes, even variable ones depending on conditions, such as local time, are obtained by different model studies [e.g., *Summers and Strobel*, 1996; *Wong and Smyth*, 2000]. For simplicity, we use a circular exobase at an altitude of 300 km above Io's surface.

We start particles along a circle in the equator of Io defined by the great circle of field lines tangential to the surface. Here we assume no longitude dependence of the $SO^+$ generation rate from a uniform SO background [*Wong and Smyth*, 2000]. In each time step a number of new $SO^+$ ions are input randomly along the source circle. Since we are performing a kinematic simulation and not a dynamic one, the number of particles followed is chosen only to be large enough to give a statistically significant picture and not to reproduce the mass of the torus. These new ions are assumed to be created in the initial ionization step. Compared with the usually high ion velocity after acceleration in the corotation electric field, the initial ion velocity disturbances, such as those from thermal velocity distribution, are much smaller. It is possible that charge-exchange ionization with torus ions can produce ions with a higher speed, but as discussed in section 3.2.1, the contribution from this process is usually smaller than that from electron impact ionization, which only causes small velocity changes during SO ionization. Also considering the fact that photoionization does not change ion velocity in a significant way, we can safely assume zero initial ion velocity.

The characteristic lifetime of the newly born $SO^+$ is $\tau_{SO^+,1}$. The Monte Carlo method is used to implement the occurrence of the neutralization reaction on the test particles in the simulation. As discussed in section 3.1, in the case of much quicker dissociation than neutralization, the effective lifetime of $SO^+$ is mainly determined by the dissociation lifetime, which can be the fastest loss mechanism of $SO^+$. Near the exobase the lifetime of $SO^+$ can be well below 1 hour because there are high torus electron and neutral densities to deplete $SO^+$. In our simulation we choose $\tau_{SO^+,1} = 20\ T_c$. Here $T_c$ is the gyroperiod of $SO^+$ and is ~1.6 s at the background magnetic field of 2000 nT near Io as used in our model calculation. Different values of $\tau_{SO^+,1}$ will be tested in section 4.3 to see its effect on SO mass loading.

Once an SO molecule is ionized, the newly born ion feels the force of the electromagnetic field and gravity fields from Io and Jupiter. The equations of ion motion can be written as

$$\frac{d\mathbf{x}}{dt} = \mathbf{v} \tag{4}$$

$$m_i \frac{d\mathbf{v}}{dt} = e(\mathbf{E} + \mathbf{v} \times \mathbf{B}) - G\frac{M_J m_i}{r_J^2}\hat{\mathbf{r}}_J - G\frac{M_I m_i}{r_I^2}\hat{\mathbf{r}}_I. \tag{5}$$

Here $\mathbf{v}$ is the particle velocity, $\mathbf{E}$ and $\mathbf{B}$ are the corotation electric field and Jupiter magnetic field at the ion's location, $G$ is the gravitational constant, $M_J$ is the mass of Jupiter, $M_I$ is the mass of Io, $r_J$ is the distance between the center of Jupiter and ion, $r_I$ is the distance between the center of Io and ion, $\hat{\mathbf{r}}_J$ is the unit vector from Jupiter center to ion, $\hat{\mathbf{r}}_I$ is the unit vector from Io center to ion, and $m_i$ is the mass

of $SO^+$. Here we do not use the drift velocity of particle in electromagnetic field, $\mathbf{v}_d = \mathbf{E}\times\mathbf{B}/B^2$, but follow the kinetic motion of the particles.

After an $SO^+$ ion is neutralized, only the gravity forces from Jupiter and Io act on the neutral particle. Equation (5) becomes

$$m_i\frac{d\mathbf{v}}{dt} = -G\frac{M_J m_i}{r_J^2}\hat{\mathbf{r}}_J - G\frac{M_I m_i}{r_I^2}\hat{\mathbf{r}}_I. \quad (6)$$

Neutral particles will be reionized after some time. We denote the characteristic lifetime of SO by $\tau_{SO}$. Since the dissociation of SO occurs over a large spatial range, the dissociation rate varies greatly with location. Near the exobase the lifetime of SO can be well less then 1 hour because of the high-density plasma and neutral that react with SO to deplete it. Very far away from Io, photoionization becomes dominant, and then a large lifetime of SO of the order of 1000 hours occurs. The lifetime used in the model should be some value between these two values. Here we choose $\tau_{SO} = 1000\ T_c$. Different values of $\tau_{SO}$ will be tested in section 4.3 to see its effect on SO mass loading.

After the particle is reionized, the ion's motion will again be controlled by (4) and (5). Since no further neutralization is considered after reionization in the model because of the usually low neutral and plasma density far away from Io, we do not need to keep the detailed information of ion motion as we did in the first-step ion trajectory calculations. At the same time, the gravity force is usually orders of magnitude smaller than the electromagnetic force. $SO^+$ will have already dissociated long before gravity exerts major influence on ion motion, and thus we can neglect the gravity force at this stage. Thus only the drift motion of the charged particles in the electromagnetic field along Jovicentric circles needs to be considered.

In our model, the final $SO^+$ ions will eventually be dissociated, with a characteristic lifetime of $\tau_{SO^+,2}$. Different from the case of $\tau_{SO^+,1}$, impact dissociation is less important because of the usually much lower electron density. Since the photodissociation is basically unchanged, we can see that $\tau_{SO^+,2}$ should be much larger than $\tau_{SO^+,1}$. Here in simulation we take $\tau_{SO^+,2} = 500\ T_c$. Different values of $\tau_{SO^+,2}$ will be tested in section 4.3 to see its effect on SO mass loading.

In the model simulation, for neutralization and reionization, we assume all the particles are transferred to SO and $SO^+$, respectively. Assuming 5% of the $SO^+$ is neutralized and the same ratio of SO is reionized in reality, the densities of SO and $SO^+$ are overestimated by factors of 20 and 400, respectively, in the model. This has to be considered when we are trying to make quantitative comparison between model results and observations. However, if we assume constant branching ratio between neutralization/reionization and other loss mechanisms at all locations, the relative density profile and global geometry of loading particles will be unchanged.

In the calculations presented here, we set $B_0 = 2000$ nT, $R_{Io} = 4.216\times10^5$ km, Io's orbit velocity around Jupiter = 17.3294 km $s^{-1}$, $M_J = 1.9\times10^{27}$ kg, $M_I = 8.94\times10^{22}$ kg, $G = 6.67\times10^{-11}$ $m^3$ $kg^{-1}$ $s^{-2}$, and Jupiter's system III period = 9 hours 55 min. The Crank-Nicholson implicit differentiation scheme is used to evolve particle motion equations (4) and (5), or (4) and (6), with an accuracy of $(\Delta t)^3$, where $\Delta t$ is the time step of simulation. For the time step we used in our calculation, 0.1 $T_0$, where $T_0$ is the normalization factor of time (in our case, $T_0 \approx 0.25$ s), this scheme produces quite accurate results for the two ion lifetimes of $\tau_{SO^+,1} = 20\ T_c$ and $\tau_{SO^+,2} = 500\ T_c$, where $T_c$ is the gyroperiod of $SO^+$ in the 2000 nT background magnetic field and $T_c = 6.28\ T_0 \approx 1.57$ s. Even for longer ion lifetimes, $\tau_{SO^+,1} = 80\ T_c$ and $\tau_{SO^+,2} = 2500\ T_c$, the error is still small enough not to significantly affect the simulation results. In order to avoid a nonphysical strip distribution of the neutral cloud in space, we input particles randomly in time within each time step instead of inputting them simultaneously.

Figure 2 shows the coordinate systems used in this study. The torus and Io rotate in a counterclockwise direction around Jupiter. Jovicentric inertial coordinates are used in the simulation. Large-scale particle propagation patterns will also be shown in this coordinate system. However, in order to compare model results with different configurations, a coordinate system moving with Io is also used, in which $\mathbf{x}$ is in the Io rotation direction and $\mathbf{y}$ is pointing to Jupiter. The $\mathbf{z}$ directions in the two coordinate systems are all outward perpendicular to the page. The magnetic field used in the calculation is in the $-\mathbf{z}$ direction, and corotation electric field $\mathbf{E}$ is always radially outward from Jupiter. Since we do not tilt the Jovian dipole in this calculation, we do not consider motion along the magnetic field.

## 4. Model Simulation Results

### 4.1. Basic Evolution of the Model and the Effects of Different Factors

**4.1.1. Case 1.** We first present the simple case of a planar $SO^+$ source. The plasma flow is uniform and in the positive $\mathbf{x}$ direction. The spatially uniform magnetic field and the corotation electric field are in the negative $\mathbf{z}$ and negative $\mathbf{y}$ directions, respectively. The characteristic lifetime of new $SO^+$ used here is $\tau_{SO^+,1} = 20\ T_c$. In this calculation, no reionization of SO neutrals and the later dissociation of $SO^+$ are included and all particles touching the source plane are considered lost. The strength of the planar source is 40 $SO^+$s $s^{-1}$ in this Monte Carlo particle simulation, and the size of the source region is 2 $R_{Io}$.

Figure 3 shows the time evolution of the particle spatial distribution for this case. At the beginning the particles

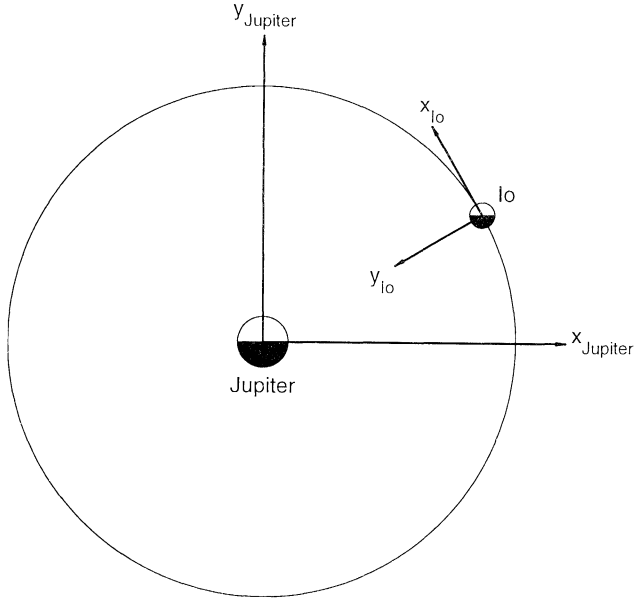


**Figure 2.** Coordinates used in the paper. Jupiter inertial coordinates are used for all the model calculations. Some of the results are shown in the Io moving coordinates for the convenience of comparing model results with observations and between different configurations.

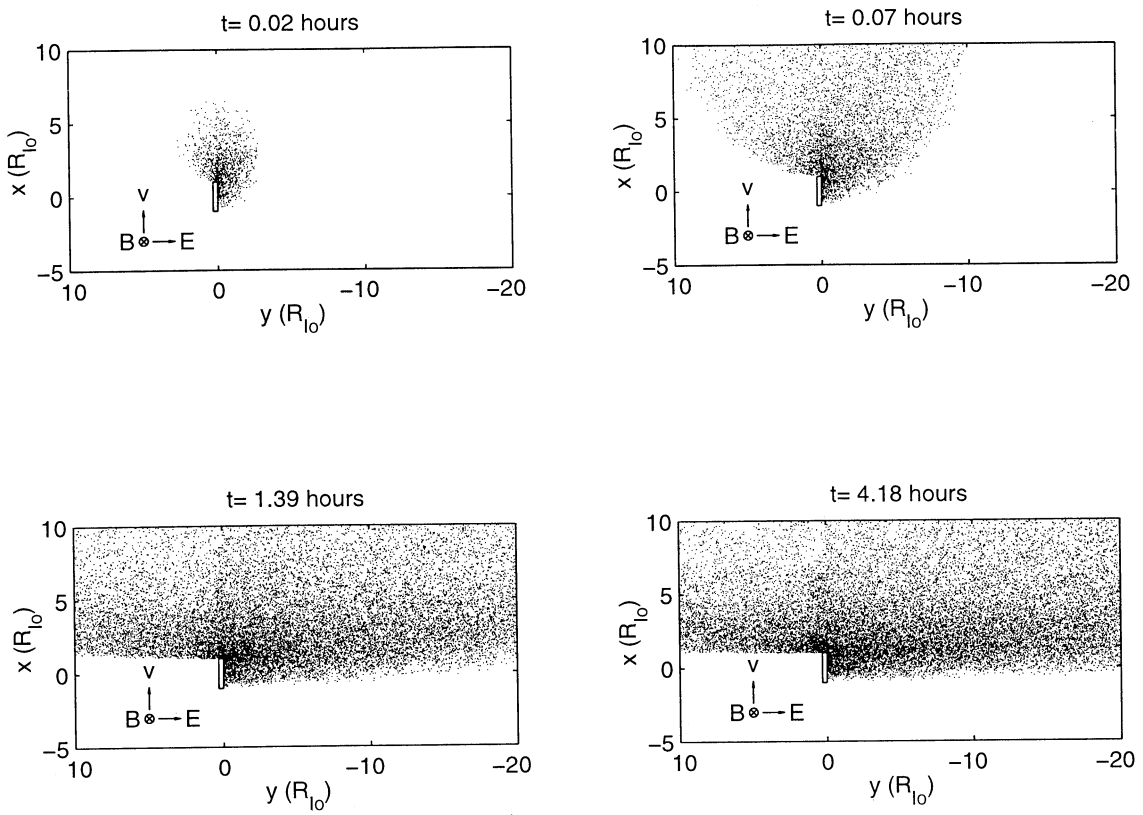


**Figure 3.** Neutral particle distributions for a 40 $SO^+$ ions $s^{-1}$ source uniformly distributed along a planar source. Results are shown at four times: $t$ = 0.02, 0.07, 1.39, and 4.18 hours. Here we use a characteristic ion lifetime of $SO^+$, $\tau_{SO^+,1} = 20\ T_c$, where $T_c$ is the gyroperiod of $SO^+$ in a magnetic field of 2000 nT. No neutral particle reionization and later dissociation are considered in this case.

propagate in various directions and form a cloud structure in space. Two boundary lines are formed in the lower right and lower left of each panel, which separate the regions with and without particles. At later times, these boundary lines become more distinct and move lower. Eventually, they are almost perpendicular to the source. In the region at the right side of the plane that is almost perpendicular to it, a high particle density structure can be seen. Note that there is also a small, high-density structure starting from the top end of the source plane extending to the left. Another less distinct high-density tail is seen from the top end of the source plane upward. These characteristics of the final particle spatial pattern can be explained by the source geometry and the lifetime distribution of new ions. For example, since we are using exponential ion neutralization loss, more particles are lost near the plane than far away from it. Meanwhile, more particles are moving quasi-perpendicularly to the source plane with lower speed than those moving in a large angle from the perpendicular direction with higher speed.

**4.1.2. Case 2.** The results of a more realistic case with a circular source are shown in Figure 4. All the other settings are the same as those used in case 1.

The spatial distribution pattern is similar to case 1. At the very beginning a small structure forms in the region on the top and to the right of the circle. As time goes on, the structure expands significantly in both **y** directions and the positive **x** direction. More pronounced gradients are formed at $t$ = 4.18 hours. Still there are two boundaries that separate regions with and without particles. The right boundary expands downward to the right, becoming almost parallel to the y-axis, with its left end attached to the bottom point of the source. The left boundary expands in the negative **x** and positive **y** directions and finally it becomes almost parallel to the y-axis, with its right end attached at the top of the source circle. After some time from the beginning, a high-density band is formed, which extends in both y directions with its bottom boundary attached to the top of the source circle. Outside the high-density band in the positive **x** direction, the particle density is lower and more uniform. No distinct high-density neutral tail exists in the downstream direction as seen in case 1. Also, there is a low-density band below the high-density band to the right of Io. The differences between the structures of case 1 and case 2 come from the changing of the source geometry. There are no particles to the left of the source circle, because after new ions are generated in this region, they are accelerated toward the the source circle and are lost there. Also, the curvature of the circle in the lower right part of the circle also damps the loading particles significantly in this case. The upper structure of the loading neutral is contributed by the upper left and upper right source region and slightly from lower right region. Since there is not much difference between the source in upper left and upper right, we can expect the disappearance of the upward tail as seen in case 1, and more similar structures on the left and right side of Io. Also, because of the stronger source at the right side of Io, we expect higher density at that side.

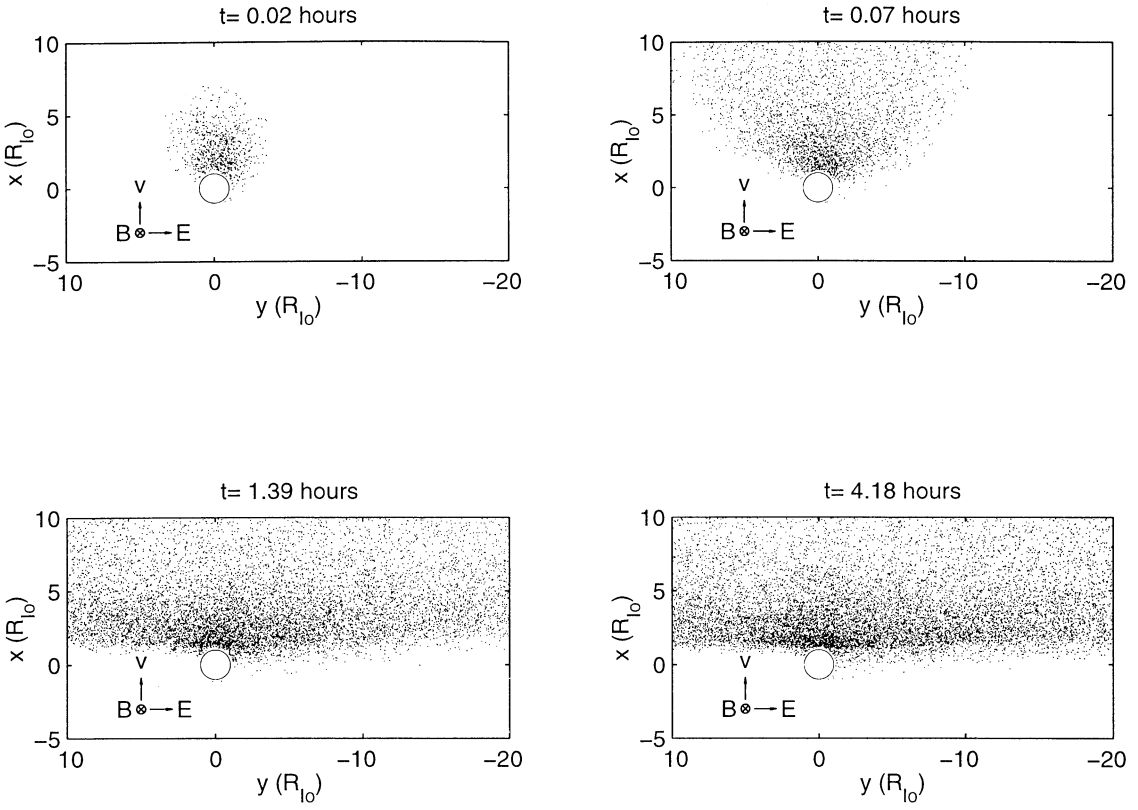


**Figure 4.** Neutral particle distributions for a 40 $SO^+$ ions $s^{-1}$ source uniformly distributed around a circle. Results are shown at four times: $t$ = 0.02, 0.07, 1.39, and 4.18 hours. Here we use a characteristic ion lifetime of $SO^+$, $\tau_{SO^+,1}$ = 20 $T_c$. No neutral particle reionization and later dissociation are considered in this case.

**4.1.3. Case 3.** Cases 1 and 2 show us the properties of the mass-loading disk due to the absorption of ions by Io and the source geometry. We now examine the effect of gravity. This time the new ions are generated in a moving frame because of the circular motion of Io around Jupiter. Meanwhile, we use a more realistic dipole magnetic field centered on Jupiter to replace the uniform magnetic field. The electric field is obtained by $\mathbf{E} = -\mathbf{v} \times \mathbf{B}$, where the corotation velocity $\mathbf{v}$ is proportional to the radial distance from Jupiter. The magnetic field changes like a dipole field to a first-order approximation. The source ring is 300 km above the Io surface on the Io equatorial plane, and particles going below 280 km altitude are considered lost. The source and loss altitudes are maintained in later sections unless explicitly stated. All the other settings are the same as those used in case 2.

The results of this case are shown in Figure 5. In order to compare the results with our former results we use an Io moving frame for display. From the figure we can see the time evolution of the loading particle distribution and the large-scale characteristics are similar to those in case 2, but important differences exist. One of them is that the final steady right boundary bends in the negative $\mathbf{x}$ direction, and the left boundary bends in the positive $\mathbf{x}$ direction. This can be seen clearly at $t$ = 1.39 hours and can be explained by the conservation of particle angular momentum in Jupiter's gravity field. At later times ($t$ = 4.18 hours) the expansion of both boundary lines masks this trend significantly. Also, the high-density beam structure extending from the top of Io becomes more diffusive. The density decreases much more quickly in the negative $\mathbf{y}$ direction along the high-density structure to the right of Io, and it is very difficult to distinguish this structure when y is beyond -15 $R_{Io}$. Io's gravity field also plays a role in producing the differences between cases 2 and 3. Especially it drags the particle motion closer to downstream direction, which helps the diffusion of the high-density structure in case 2. It also enforces the bend at the left side of Io and weakens the bend on the other side.

**4.1.4. Case 4.** In cases 1–3 we have included what we feel are the most important factors in determining the structure of the mass-loading disk, but we have not yet addressed the reionization of SO neutral particles and the later dissociation of $SO^+$. As we discussed in section 3.2.3, after a neutral particle travels for some time, it will eventually be reionized by impact ionization, charge exchange, or photoionization. Meanwhile, near Io the plasma ion cyclotron wave observations are directly related to the ion distribution [*Russell et al.*, this issue]. In this test case we include the finite neutral ionization rate and $SO^+$ dissociation rate to calculate the neutral and ion distributions. The characteristic lifetimes for initial ions, neutral ions, and final ions are $\tau_{SO^+,1}$ = 20 $T_c$, $\tau_{SO}$ = 1000 $T_c$, and $\tau_{SO^+,2}$ = 500 $T_c$. A constant source of 160 $SO^+$ ions $s^{-1}$ is added uniformly along the circular source. The other parameters are the same as those used in case 3.

When we include the neutral loss rate, there are no significant changes in the spatial distribution of the SO neutrals, since $\tau_{SO}$ is large and the production rate of $SO^+$ is low. Still, however, observable changes exist, as shown in Fig-

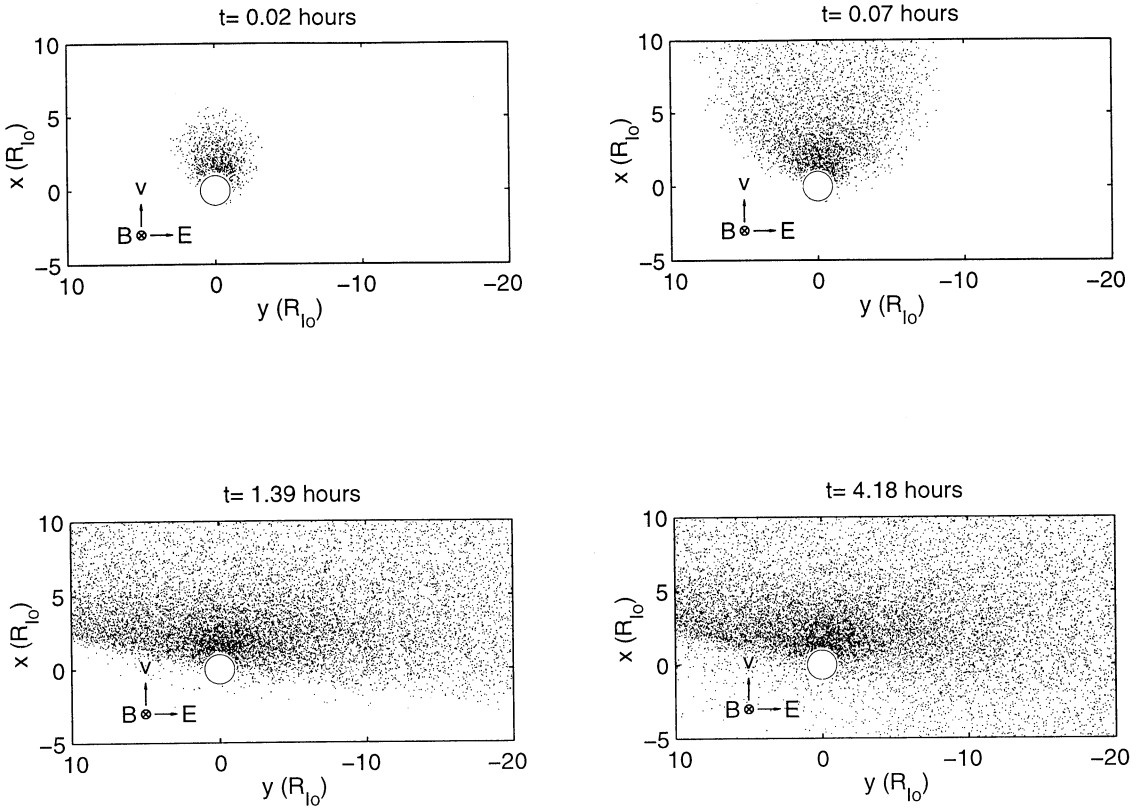


**Figure 5.** Solutions in Figure 4 repeated using the gravitational fields of Jupiter and Io. Radially varying magnetic field and corotation electric field are also included in the calculation. Results are shown at four times: $t$ = 0.02, 0.07, 1.39, and 4.18 hours. Here we use a characteristic ion lifetime of $SO^+$, $\tau_{SO^+,1} = 20\ T_c$. No neutral particle reionization and later dissociation are considered in this case.

ure 6. Because of the loss of SO by ionization, a lower SO density is obtained than that in case 3. Meanwhile, sharper lower boundary lines are formed than the much more diffuse ones in the former case. We believe the diffuse boundaries in case 3 are formed by low-speed neutrals, which are usually lost before they can propagate farther. Also, a uniform downstream distribution is obtained without a distinguishable high-density tail.

Figure 7 shows the evolution of the $SO^+$ spatial distributions in this case. The ion distribution experiences an expansion phase similar to its neutral counterpart and eventually forms a stable structure with two boundary lines, reflecting the neutral distribution as its source. Because of the high neutral density near the wake region of Io, a high-density ion tail is formed upward from the top of Io. Also, different from case 3 showing the SO distribution, there is a very obvious $SO^+$ asymmetry across Io's trajectory downstream of Io. On the anti-Jupiter side of the Io trajectory, the $SO^+$ density is higher than that on the Jupiter side. The reason is that there is higher neutral density on the anti-Jupiter side of Io than on the other side.

## 4.2. Large-Scale Io Mass-Loading Pattern

Above, we have presented the basic elements of the model. Although the simulations are performed in the Jupiter inertial frame, all the results are shown in the Io frame. At the same time, the calculations are constrained to small regions near Io. In this section we examine the global structure resulting from the model. All the particle spatial distribution results in this section are shown in the Jupiter inertial frame.

Two loss boundaries are used, out of which particle trajectories are no longer followed. The inner boundary is the surface of Jupiter and the outer boundary is a circle with a radius of 11.8 $R_J$, twice as long as the distance between Io and Jupiter. No particles reach the inner boundary for the parameters we choose, but there are a few particles that reach the outer boundary in this case. Considering the usually very small particle density near the boundary, the loss of particles is negligible. A uniform particle input flux rate of 40 particles $s^{-1}$ is used. The other parameters are the same as those in case 4.

Figure 8 shows the evolution of the large-scale SO distribution. At the beginning of the simulation, SO forms a cloud that expands in space with time. By $t$ = 2.78 hours, the spatial pattern of the neutral particles begins to become steady and there is very little change even at time $t$ = 6.96 hours. Io is orbiting anticlockwise around Jupiter, and the neutral cloud rotates with it, seemingly fixed to it when it reaches its steady state. The structure of the neutral cloud is similar to the sodium cloud structure obtained by *Smyth* [1979]. The most important difference between these two structures is that in the latter model, mass-loading particles can expand to the region of the torus upstream from Io. Thus Io is in the middle of the mass-loading cloud. However, in our model, because of the large torus corotation velocity and the electromagnetic field configuration we used, no upstream particles exist. Thus Io is at the upstream boundary of the mass-loading region, which is consistent with the I24 and I27 Galileo ion cyclotron wave observations near Io with a sharp increase in wave power between upstream and downstream of Io [*Russell et al.*, this issue].

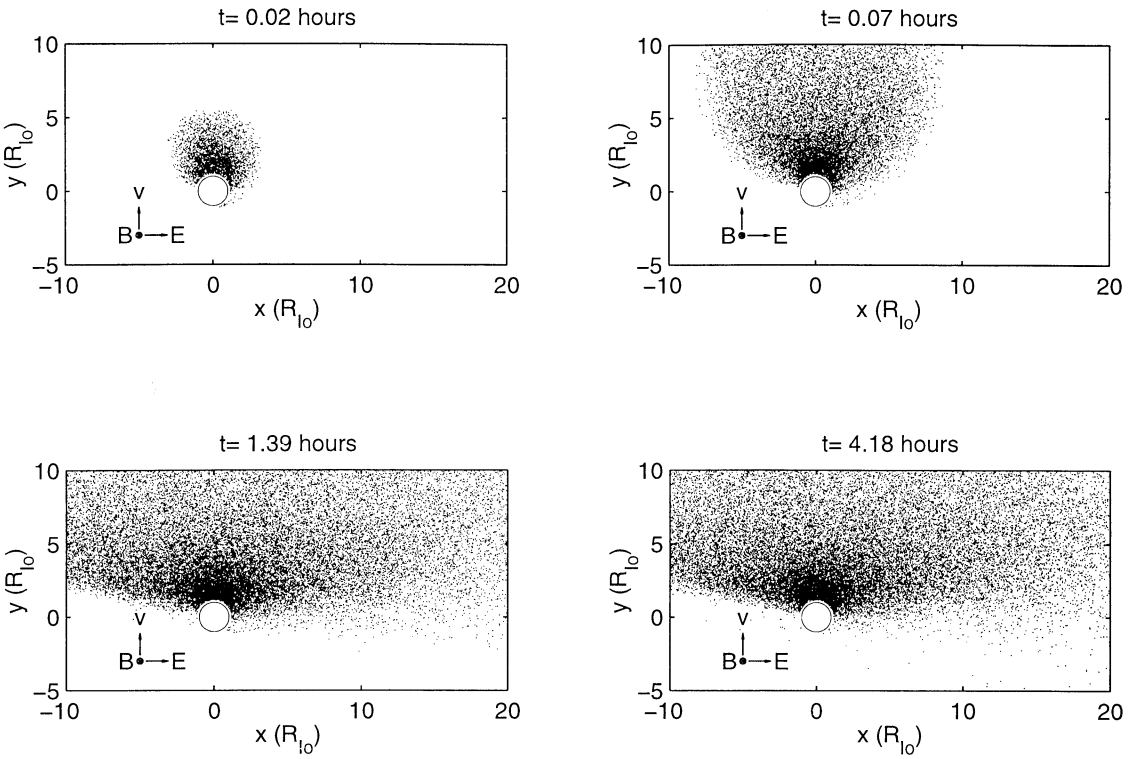


**Figure 6.** SO distributions at different times $t$ = 0.02, 0.07, 1.39, and 4.18 hours with the consideration of SO reionization and later $SO^+$ dissociation. Here we use $\tau_{SO^+,1} = 20\ T_c$, $\tau_{SO} = 1000\ T_c$, and $\tau_{SO^+,2} = 500\ T_c$. A source of 160 $SO^+$ ions $s^{-1}$ is used in the calculation. All the other parameters are the same as those in case 3.

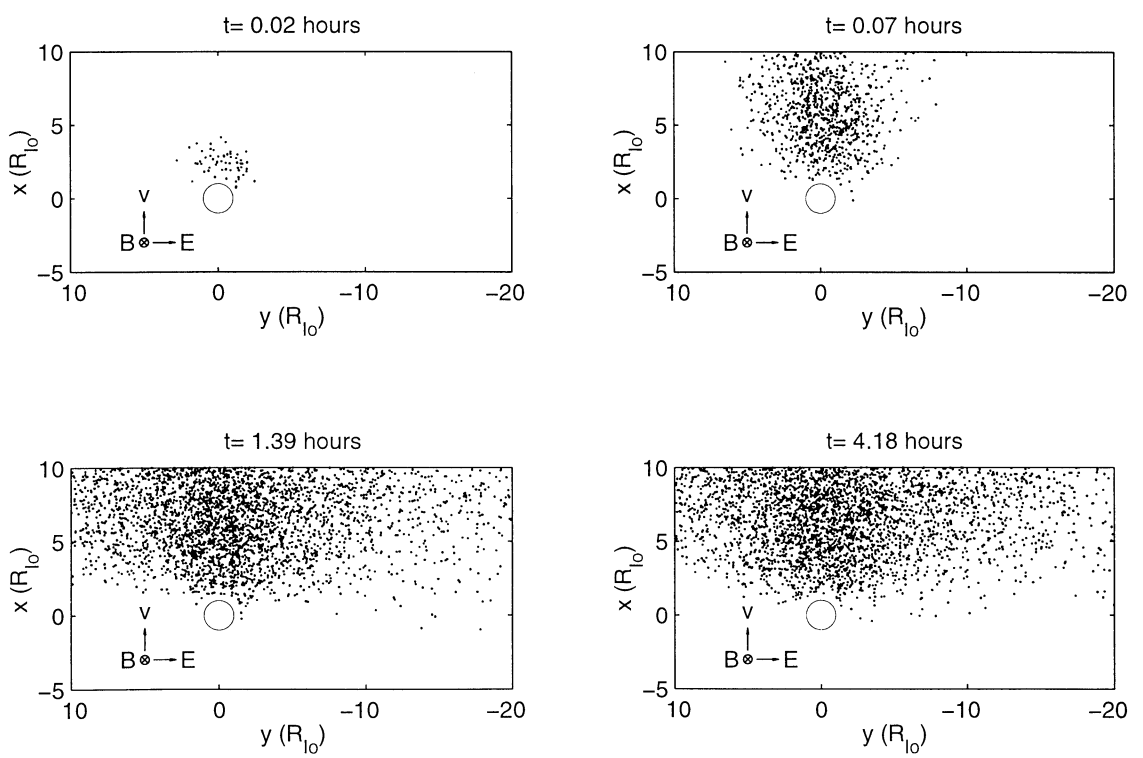


**Figure 7.** $SO^+$ distributions at different times $t$ = 0.02, 0.07, 1.39, and 4.18 hours with the consideration of SO reionization and later $SO^+$ dissociation. Here we use $\tau_{SO^+,1} = 20\ T_c$, $\tau_{SO} = 1000\ T_c$, and $\tau_{SO^+,2} = 500\ T_c$. A source of 160 $SO^+$ ions $s^{-1}$ is used in the calculation. All the other parameters are the same as those in case 3.

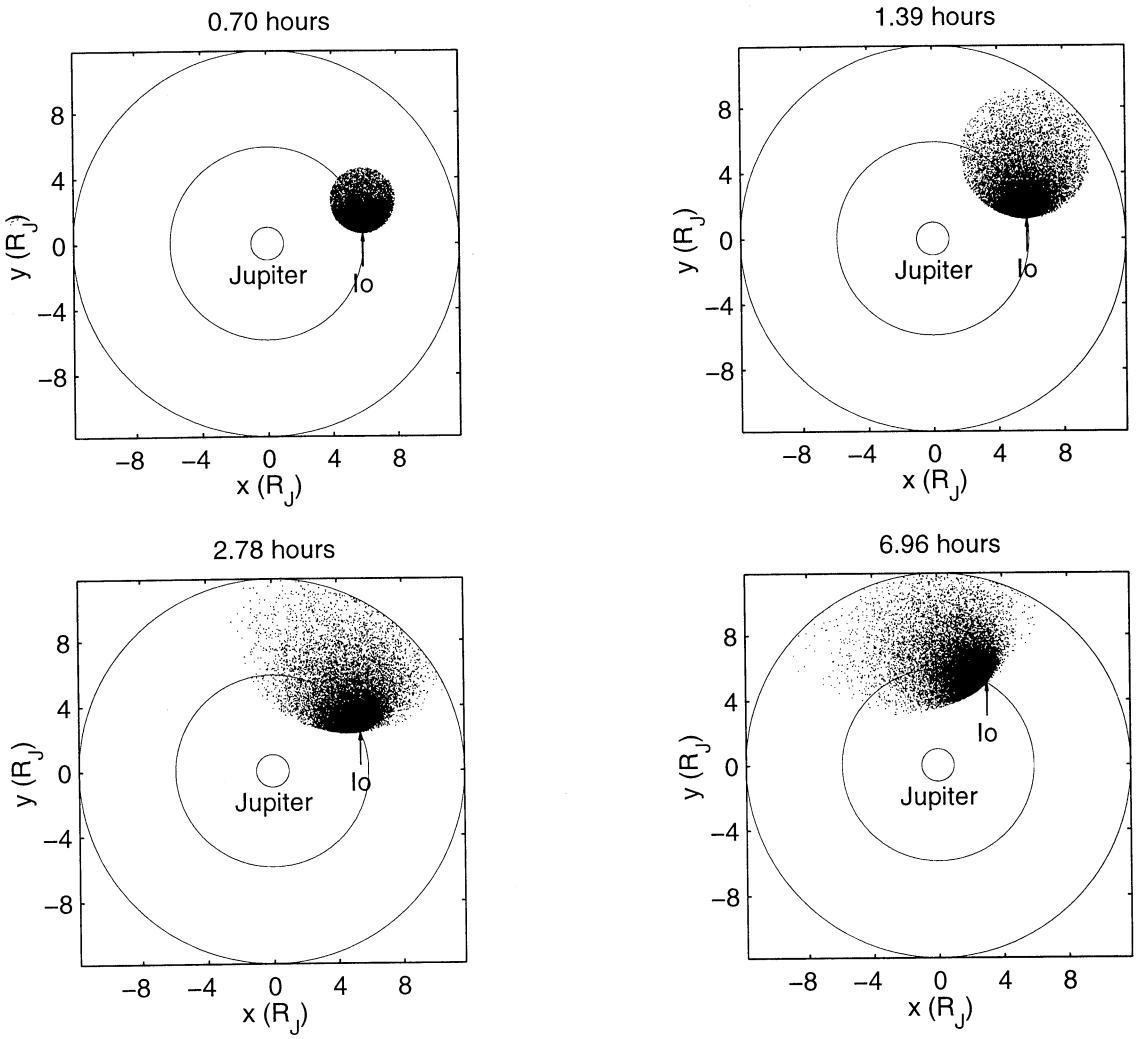


**Figure 8.** Large-scale evolution of Io neutral SO spatial distribution. Neutral distributions at four times are shown: $t = 0.7$, 1.39, 2.78, and 6.96 hours. Here $\tau_{SO^+,1} = 20\ T_c$, $\tau_{SO} = 1000\ T_c$, and $\tau_{SO^+,2} = 500\ T_c$. The inner boundary of the simulation is the surface of Jupiter, and the outer boundary is 2 times the distance from Io to Jupiter. Uniform input flux of 40 $SO^+$ ions $s^{-1}$ from Io source circle is used.

Figure 9 shows the evolution of the large-scale $SO^+$ distribution. At the beginning, $SO^+$ forms a cloud and expands in space with time. By $t = 2.78$ hours, the spatial pattern of the ions becomes steady and there is very little change even at time $t = 6.96$ hours, which is consistent with SO evolutions. For the parameters we used in this case, it is difficult to see the differences between neutral and ion distributions in Figures 8 and 9, though the stretching effect of the neutral clouds of Figure 8 is shown in the ion clouds of Figure 9. The enlarged figures of stable neutral and ion distributions at $t = 6.96$ hours are shown in Figure 10, from which a more distinct difference between these two distributions can be seen. Note that in the ion plot, there is an asymmetric torus-like structure with high ion density along the Io trajectory that extends radially inward and outward. Another important feature for the neutral distribution in Figure 10 is the obvious directional feature; that is, a neutral structure extends radially inward and outward from Io. More neutrals are loaded outside of the Io trajectory than inside as a result of the configuration used in our model. Instead of forming a purely perpendicular structure, the directional feature of the model neutral cloud has its own special pattern, in which a large bend exists inside the Io trajectory and there is little bend outside.

The radial mass-loading profile of the steady particle distribution is shown in Figure 11. From the figure we can see that there is an obvious density peak near the Io orbit. The density decreases sharply away from the peak, and the profile is not symmetric about the peak. The density inside the peak drops more quickly than that outside, which is consistent with the Galileo I0 observation that there is higher density outside the Io orbit than inside [*Bagenal et al.*, 1997]. In this case, there is an inner boundary for torus particles at a Jovicentric radius of about 3.4 $R_J$, which is mainly caused by Jupiter gravity. At the outer boundary the density is not zero but is small compared with the peak value.

In order to obtain the velocity distribution of the steady pattern of the torus particles in the simulation, we proceeded as follows. First we obtained the velocity of ions in the simulation. Then we removed the drift velocity from the

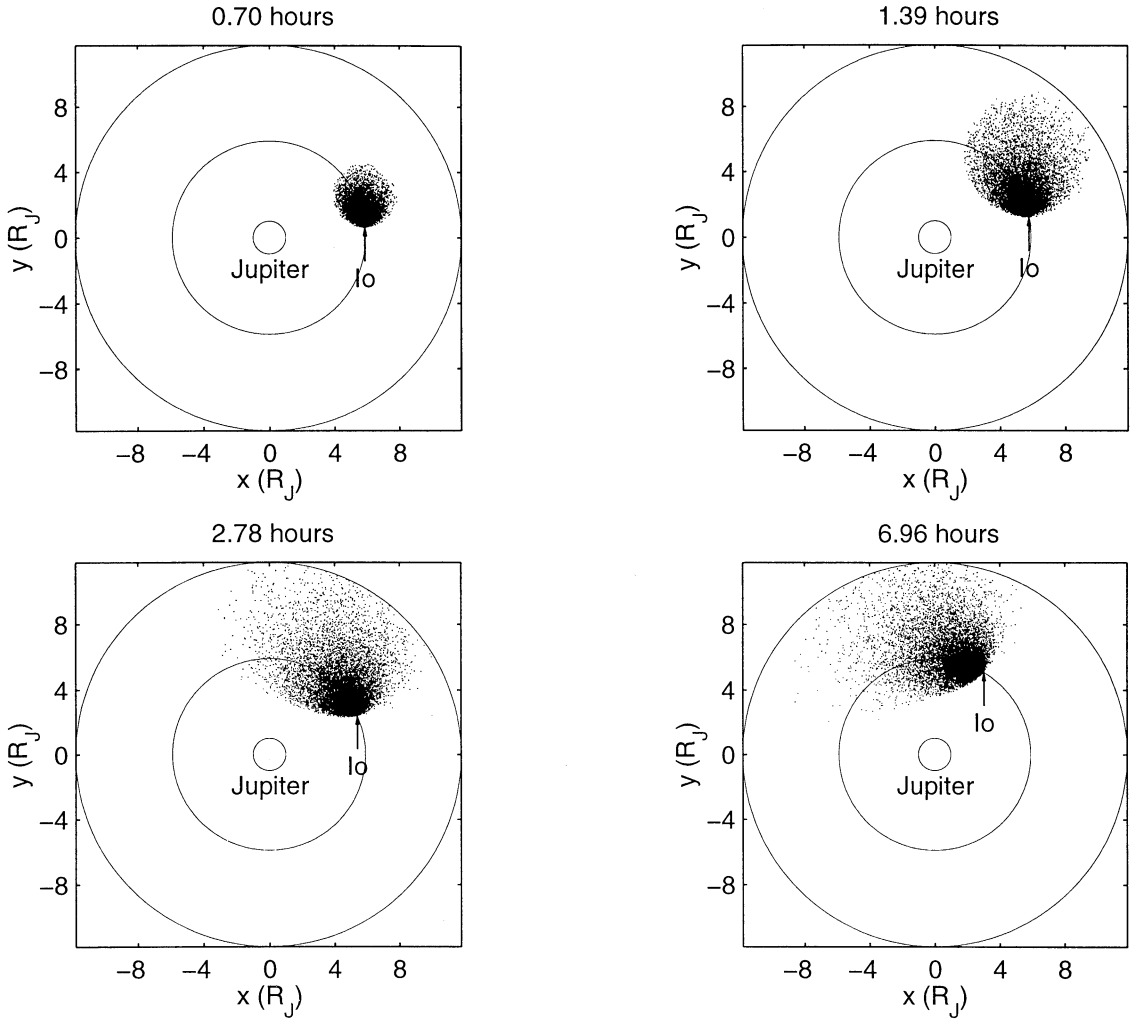


**Figure 9.** Large-scale evolution of $SO^+$ spatial distribution. Ion distributions at four times are shown: $t$ = 0.7, 1.39, 2.78, and 6.96 hours. Here $\tau_{SO^+,1} = 20\ T_c$, $\tau_{SO} = 1000\ T_c$, and $\tau_{SO^+,2} = 500\ T_c$. The inner boundary of the simulation is the surface of Jupiter, and the outer boundary is 2 times the distance from Io to Jupiter. Uniform input flux of 40 $SO^+$ ions $s^{-1}$ from Io is used.

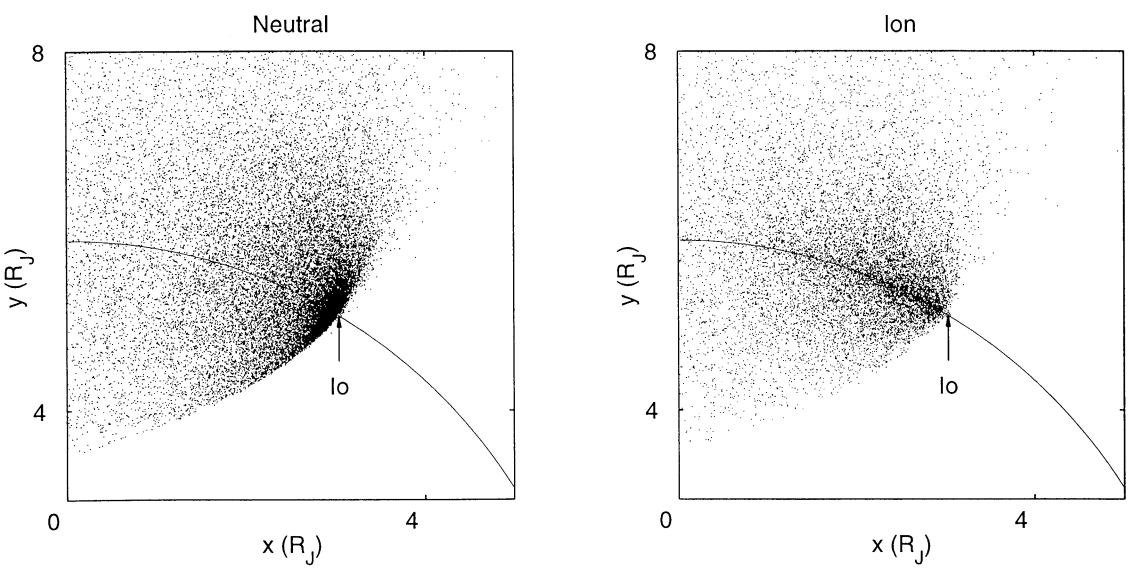


**Figure 10.** Detailed structure of the steady neutral and ion distribution shown in Figure 8 and Figure 9 at $t$ = 6.96 hours. We can see clearly the difference between neutral and ion distribution. An ion distribution with $SO^+$ peak density near the Io orbit and its wide extension inward and outward corresponds well with Io torus observations.

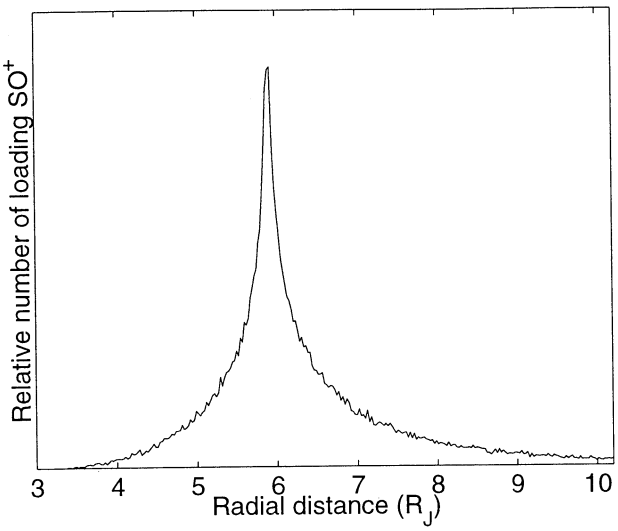


**Figure 11.** Radial profile of loading particles for the steady state at $t = 6.96$ hours in Figure 9.

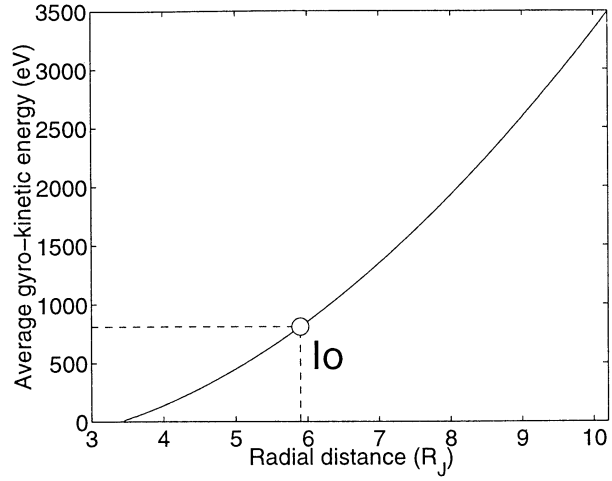


**Figure 12.** Average gyrokinetic energy radial profile for the stationary ion distribution at $t = 6.96$ hours. We can see that the average gyrokinetic energy increases monotonically with radial distance from Jupiter. Near Io the average gyrovelocity is about 57 km $s^{-1}$, which is the difference between Io and its torus velocity.

particle motion. The resulting velocity is circular in phase space, typical for pickup ions. The radius of the circle is the velocity at which the ions gyrate. The loading $SO^+$ gyrokinetic energy radial profile is shown in Figure 12. The farther away from the Jupiter, the higher the gyrokinetic energy. Thus ions outside of the Io orbit have more gyrokinetic energy and, when scattered, a higher thermal temperature can be expected than those inside Io orbit. This is qualitatively consistent with the observation that the temperature of ions is higher in the outer torus than the inner torus [*Bagenal et al.*, 1980; *Crary et al.*, 1998]. The "ring"-type distribution of newly created ions is unstable and generates the observed ion cyclotron waves [*Huddleston et al.*, 1998; *Blanco-Cano et al.*, this issue]. We can expect stronger wave power outside Io's orbit than inside because of the higher free energy outside. This helps us to link the mass-loading ion density and gyrovelocity results from our model simulation to the ion cyclotron wave observations by Galileo [*Russell et al.*, this issue]. Note the deviation of the curvature from a straight line and a gyrokinetic energy cutoff at about 3.4 $R_J$ away from Jupiter in Figure 12. These are mainly caused by Jupiter's gravity.

### 4.3. Parameter Influence on Model Results

As discussed in section 3.3, the choosing of $\tau_{SO^+,1} = 20$ $T_c$, $\tau_{SO} = 1000$ $T_c$, and $\tau_{SO^+,2} = 500$ $T_c$ is based on theoretical analysis and former study results. However, because of the complexity of the Io mass-loading process, large differences between the parameters we choose and their actual values, as well as the large variations of these parameters under different conditions, make it necessary for us to perform a parametric study to see the effects of the different parameters. In this section we vary the three major parameters of our model, $\tau_{SO^+,1}$, $\tau_{SO}$, and $\tau_{SO^+,2}$, and analyze the corresponding results. The different test parameters are listed in Table 1, where test 0 is the case with the typical parameters used in section 4.2.

Figure 13 and Figure 14 show the steady SO and $SO^+$ distributions for the different testing parameters at $t = 6.96$ hours. Changing $\tau_{SO^+,1}$ from 5 to 80 $T_c$ does not change the loading process much, and it is difficult to tell the difference between the two test results in both the neutral and ion distributions. Small differences can be seen from the mass-loading radial profile, which will be discussed shortly. However, changing $\tau_{SO}$ from 200 to 5000 $T_c$ causes significant changes to the mass loading. The neutral and ion spatial distributions are much different from each other and from the former typical parameter results. Specifically, when $\tau_{SO}$ is small (200 $T_c$), very small scale neutral loading is formed. This is easy to understand because of the fast ionization of the neutrals. Correspondingly, the distribution of ions is restricted to a small radial range but with much higher density, since we are using the same source rate in all the cases. When $\tau_{SO}$ is large (5000 $T_c$), a huge neutral structure forms, with the most upstream extending boundary among all the test results. The structure extends well outside of the outer boundary of the calculation. Thus only a limited portion of the particles are loaded within this range, which can be seen from the low ion density in Figure 14. Such a large structure is inconsistent with observations. Since the neutral pattern is only controlled by $\tau_{SO^+,1}$ and $\tau_{SO}$, it is not a surprise that we obtained the same neutral distribution in tests 5 and 6 as that in test 0. However, unlike a typical parameter study, much different $SO^+$ distributions are obtained from the same neutral distribution for $\tau_{SO^+,2} = 100$ $T_c$ and $\tau_{SO^+,2} = 2500$ $T_c$. When $\tau_{SO^+,2}$ is small (100 $T_c$), $SO^+$ ions from the reionization process are dissociated quickly before they form a large $SO^+$ tail. However, when $\tau_{SO^+,2}$ is large, long tails of $SO^+$ can form.

Though Figures 13 and 14 can give a clear view of the neutral and ion loading geometries for different parameters,

**Table 1.** Test Parameters

| Test Number | $\tau_{SO^+,1}$, $T_c$ | $\tau_{SO}$, $T_c$ | $\tau_{SO^+,2}$, $T_c$ |
|---|---|---|---|
| 0 | 20 | 1000 | 500 |
| 1 | 5 | ... | ... |
| 2 | 80 | ... | ... |
| 3 | ... | 200 | ... |
| 4 | ... | 5000 | ... |
| 5 | ... | ... | 100 |
| 6 | ... | ... | 2500 |

[a]Ellipsis dots mean the parameter is the same as the typical parameter in test 0.

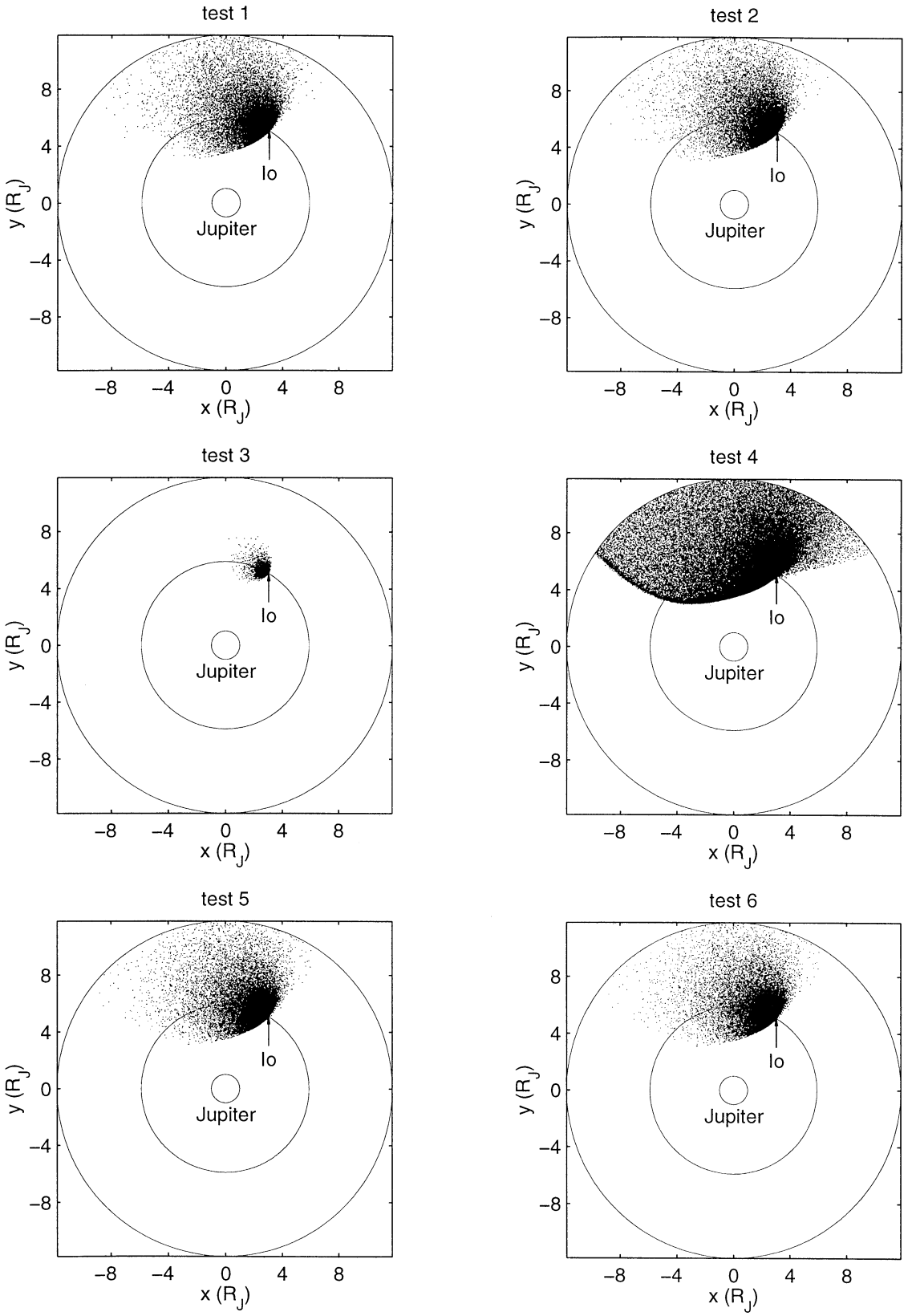


**Figure 13.** Stable model neutral distribution obtained with different parameters of $\tau_{SO^+,1}$, $\tau_{SO}$, and $\tau_{SO^+,2}$ at $t = 6.96$ hours. Inner boundary of 1 $R_J$ and outer boundary of 11.8 $R_J$ are used in these calculations. Each Io location is shown with an arrow.

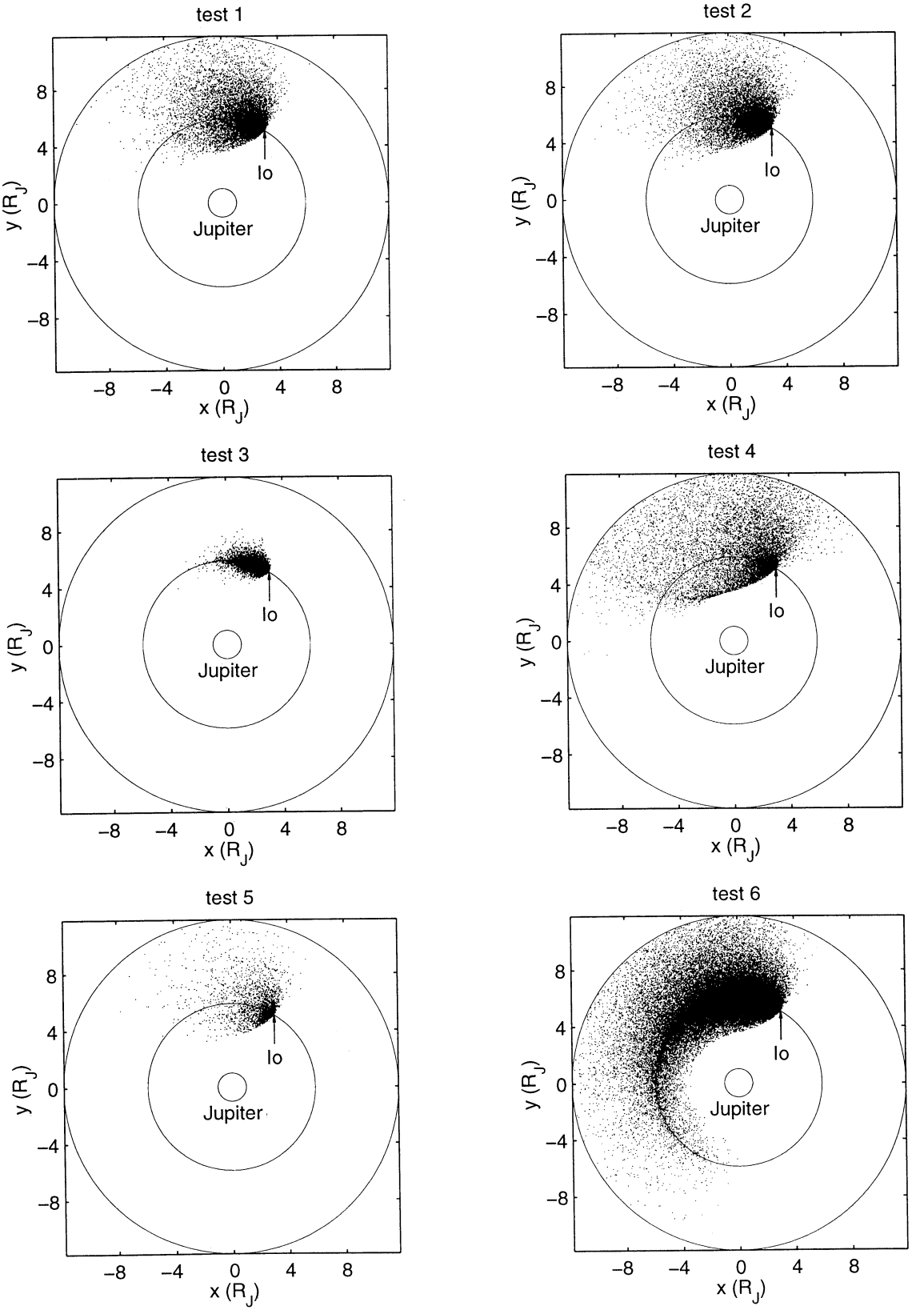


**Figure 14.** Stable model ion distribution obtained with different parameters of $\tau_{SO^+,1}$, $\tau_{SO}$, and $\tau_{SO^+,2}$ at $t = 6.96$ hours. An inner boundary of 1 $R_J$ and an outer boundary of 11.8 $R_J$ are used in these calculations. Each Io location is shown with an arrow.

it is not easy to tell the relative amount of particles loaded at different radial distances from Jupiter. Figure 15 helps us to reach this point by showing the particle loading profiles under different conditions. Small but distinct changes can be seen when we change $\tau_{SO^+,1}$ from 80 to 5 $T_c$ with constant $\tau_{SO} = 1000\ T_c$ and $\tau_{SO^+,2} = 500\ T_c$. Specifically, the peak of the loading ions moves radially outward and the peak density becomes lower. Fewer particles are loaded inside the peak, but little change happened outside. As a whole, the total number of particles loaded decreased. This is easy to understand, because when $\tau_{SO^+,1}$ is smaller, more particles can be lost into Io's atmosphere. When we change $\tau_{SO}$ with constant $\tau_{SO^+,1} = 20\ T_c$ and $\tau_{SO^+,2} = 500\ T_c$, there are significant changes. When $\tau_{SO}$ is small (200 $T_c$), a high ion peak is formed and fewer ions are emplaced far from Io. When $\tau_{SO}$ is big (5000 $T_c$), lower ion peak forms and there is a much wider radial expansion for loading ions.

## 5. Discussion

From the above results, we can see that many observational characteristics of the Io mass-loading particles can be obtained from our multistep mass-loading model. The ion radial profile is consistent with the observed Io torus peak density near the orbit of Io and the asymmetric particle density profile inside and outside of Io orbit. The decreasing particle ring gyrokinetic energy with the decreasing distance from Jupiter can contribute to the observed cold torus inside the Io orbit and hot torus outside of the Io orbit. In the model results, Io is always on the upstream boundary of the loading cloud. Usually a sharp boundary of the loading ion cloud between upstream and downstream of Io torus exists near Io. This corresponds very well with the drastic increase of observed $SO^+$ ion cyclotron waves near Io during the Galileo I24 and I27 Io flybys, when the spacecraft flew from upstream to downstream of Io torus near Io [*Russell et al.*, this issue]. This observation also eliminates the possibility that the source cloud has a banana-shaped cloud with significant densities upstream of Io. Characteristic lifetimes for ions, $\tau_{SO^+,1}$ and $\tau_{SO^+,2}$, and neutral particles, $\tau_{SO}$, are found to control the structure of the neutral disk and the resulting pattern of ion mass loading. These three lifetimes reflect the average neutralization, ionization, and dissociation over the whole mass-loading region.

In the simulation we did not consider any torus particle loss mechanism after $SO^+$ dissociation. The resulting ions drift in the electromagnetic field configuration discussed in section 3.3. As no loss mechanism of torus ions is included in the model, as time goes on, the density of charged particles will increase toward infinity in the torus, though the neutral pattern does not change (in reality, it should change with local time and Io source variations). This cannot happen in reality because of the existence of loss processes. Wave-particle interactions can produce pitch angle diffusion [*Scarf*

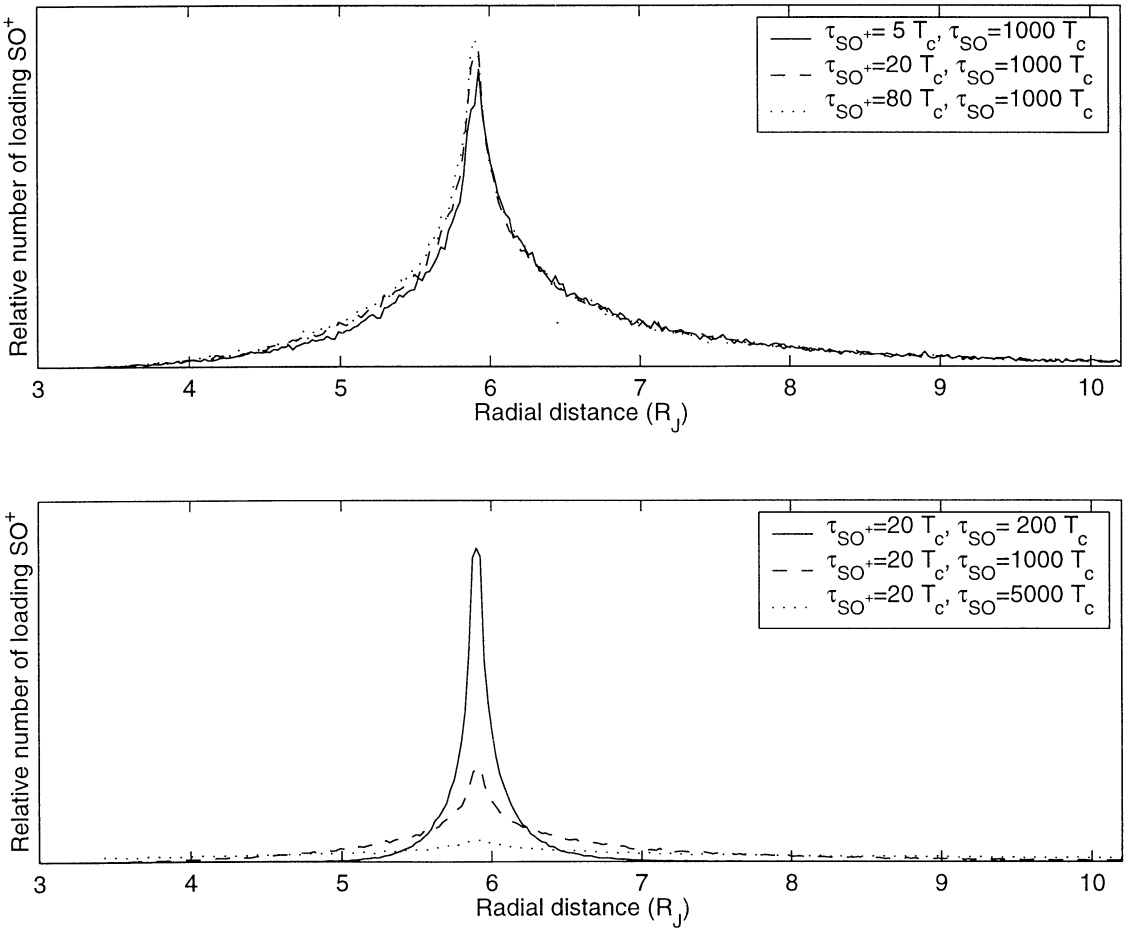


**Figure 15.** Stable ion radial loading profile obtained with different parameters of $\tau_{SO^+,1}$ and $\tau_{SO}$ at $t = 6.96$ hours. Constant $\tau_{SO^+,2} = 500\ T_c$ is used because radial loading profile does not depend on it.

*et al.*, 1979], which causes the diffusion of particles along the magnetic field into the Jovian atmosphere. If this process were not rapid enough, the density would continue to build up until centrifugal forces cause radial transport [*Russell et al.*, 2000].

In the model an ideal dipole magnetic field and a frozen-in condition electric field are used. This works well for regions some distance away from the Io surface, but for regions within about 1 $R_{Io}$ above the Io surface, the interaction between torus plasma and Io produces a flow pattern far more complex than our uniform flow, as evidenced by both observations and simulations [*Frank et al.*, 1996; *Kivelson et al.*, 1996; *Linker et al.*, 1998; *Saur et al.*, 1999]. These complex field structures will cause differences in the spatial distribution of the mass-loading particles.

Though simulation results have shown our model's ability to reproduce many features of the Io mass-loading process, large difference exists between the model's gyrokinetic energy prediction (~800 eV near Io trajectory from Figure 12) and the corresponding observation results (~1−60 eV near Io's trajectory) [*Frank et al.*, 1996; *Crary et al.*, 1998; *Russell et al.*, 2000]. Some of the gyrokinetic energy can be dissipated by wave-particle interactions. Collisions can transfer energy to the bound electrons of the torus ions and neutrals that, in turn, radiate energy into space. This radiation also cools the torus. However, it is difficult for these mechanisms to account for the very low temperature observed in the Io torus wake region immediately behind Io. Here we analyze a third possible cause for the large temperature difference, the nonuniform electric field associated with the slow flow of the flux tubes that drift across Io rather than being deflected around it. To avoid unnecessary complexity, we assume constant background magnetic field near Io. This is reasonable because the magnetic field variations near Io are usually very small ( ~10% of the background magnetic field) [*Kivelson et al.*, 1996]. If particles are picked up in the high-speed flow regions, the gyrovelocity of the pickup ion will be high. The perpendicular gyrokinetic energy $W_\perp$ will be constant from the conservation of the first adiabatic invariant, $\mu = W_\perp/B$, so the ion remains "hot" as it moves away from Io. All the calculations shown previously in this paper are for this case. However, those flux tubes that do not flow around Io, but connect to it, move very slowly across it. When the plasma flow speed in the loading region is as low as it is here, the gyrovelocity of the pickup particle will be low. When a flux tube returns to the normal corotation velocity behind Io, the small $W_\perp$ of the particle remains, from the conservation of the first adiabatic invariant, even though the bulk velocity of the plasma is the same as the surrounding torus. Thus the flux tubes that cross Io pick up cold ions, and these ions remain cold. Therefore the mass-loading process at Io simultaneously produces both warm and cold plasma with the cold plasma in the narrow wake region and the warm plasma both inward and outward from Io. Assuming that most of the particles in the near torus wake region are produced from the slow loading region, the low temperature corresponds to a loading region plasma flow velocity of about 2-16 km $s^{-1}$ for those tubes that cross Io. We expect this narrow flow region to have a relatively small effect on the overall structure of the torus.

One important implication of our study is that the mass-loading region is extensive in the down wake direction. Much of the ionic mass added to the Io torus is deposited well downstream of Io and would not be observed as freshly added ions convecting past the spacecraft on a radial pass close to Io such as the Io Galileo pass. Thus estimates like those of *Bagenal* [1997] likely underestimate the mass loading in the torus as a whole. A second almost paradoxical implication is that the momentum is transferred to the Io torus principally in the near vicinity of Io. There is certainly some momentum coupling with the ionosphere over the entire mass-loading region, but a large portion of the acceleration occurs where the fast neutrals are first produced. This helps explain why the Io flux tube is so active compared with the rest of the torus region despite the vast extent of the mass-loading region.

Io mass loading is a complex process. This is the reason why almost all the current models make many simplifying assumptions [*Summers and Strobel*, 1996; *Linker et al.*, 1998; *Wong and Smyth*, 2000]. A more realistic self-consistent model description should not only include a realistic flow past Io, Io's atmospheric and ionospheric processes, and realistic source dynamics on the Io surface, but also include the proper coupling between them. Multiscale processes exist in the mass-loading region, and they should also be included in the model description, which is challenging in terms of including the physics and in terms of the computer power required to run such simulations. The WS model and our extension to the model can be viewed as a step to connect the local Io source properties with the large-scale Io mass-loading particle propagation pattern, and the results show the strong dependence of the large-scale mass-loading pattern on the Io source and field structures.

## 6. Conclusions

The model discussed in this study extends the work of *Wilson and Schneider* [1999]. We have attempted to use this model to explain the observations of Io mass loading, especially the latest Io wave observations, and in situ density and temperature observations. In summary, we have shown the following:

1. The multistep mass-loading process can explain the mass loading of Io particles over a wide range of distances from Io. Various observational Io mass-loading particle properties, such as the loading particle directional features (neutral structure that extends almost radially inward and outward from Io), high (low) torus density outside (inside) of Io's orbit, spatial wave distribution and changing pattern near Io, and the torus plasma temperature, can be explained by this model.

2. Several factors contribute to the final mass-loading pattern, including the source geometry, gravity, and the background electric and magnetic field structures. Three parameters, namely, the characteristic lifetimes of ions, $\tau_{SO^+,1}$ and $\tau_{SO^+,2}$, and the characteristic lifetime of neutrals, $\tau_{SO}$, are found to be essential in controlling the mass-loading pattern.

3. Flux tubes that convect across Io can pick up cold ions, and these ions may contribute to the formation of the cold torus plasma.

4. Although diffusion may occur in the Io plasma torus especially at higher energies, a kinetic process, involving the cross-field transport by neutrals, is sufficient to explain many observational features.

**Acknowledgments.** We are grateful to the useful discussion with F. Bagenal, K.K. Khurana, M.G. Kivelson, and J.K. Wilson, as well as very helpful suggestions from both referees. This work was supported by the National Aeronautics and Space Administration under research grant NAG5-8938. This is IGPP publication 5491.

Hiroshi Matsumoto thanks A. Morioka and S. Machida for their assistance in evaluating this paper.

## References

Bagenal, F., Plasma conditions inside Io's orbit: Voyager measurements, *J. Geophys. Res.*, *90*, 311, 1985.

Bagenal, F., The ionization source near Io from Galileo wake data, *Geophys. Res. Lett.*, *24*, 2111, 1997.

Bagenal, F., and J. D. Sullivan, Direct plasma measurements in the Io torus and inner magnetosphere of Jupiter, *J. Geophys. Res.*, *86*, 8447, 1981.

Bagenal, F., J. D. Sullivan, and G. L. Siscoe, Spatial distribution of plasma in the Io torus, *Geophys. Res. Lett.*, *7*, 41, 1980.

Bagenal, F., F. J. Crary, A. I. F. Stewart, N. M. Schneider, D. A. Gurnett, W. S. Kurth, L. A. Frank, and W. R. Paterson, Galileo measurements of plasma density in the Io torus, *Geophys. Res. Lett.*, *24*, 2119, 1997.

Ballester, G. E., M. A. McGrath, D. F. Strobel, X. Zhu, P. D. Feldman, and H. W. Moos, Detection of the $SO_2$ atmosphere on Io with the Hubble Space Telescope, *Icarus*, *111*, 2, 1994.

Blanco-Cano, X., C. T. Russell, and R. J. Strangeway, The Io mass-loading disk: Wave dispersion analysis, *J. Geophys. Res.*, this issue.

Bridge, H. S., et al., Plasma observations near Jupiter: Initial results from Voyager 1, *Science*, *204*, 987, 1979.

Brown, M. E., Observation of mass loading in the Io plasma torus, *Geophys. Res. Lett.*, *21*, 847, 1994.

Burger, M. H., N. M. Schneider, and J. K. Wilson, Galileo's close-up view of the Io sodium jet, *Geophys. Res. Lett.*, *26*, 3333, 1999.

Crary, F. J., F. Bagenal, L. A. Frank, and W. R. Paterson, Galileo plasma spectrometer measurements of composition and temperature in the Io plasma torus, *J. Geophys. Res.*, *103*, 29,359, 1998.

Dessler, A. J., Mass-injection rate from Io into the Io plasma torus, *Icarus*, *44*, 291, 1980.

Feldman, P. D., et al., Lyman-$\alpha$ imaging of the $SO_2$ distribution on Io, *Geophys. Res. Lett.*, *27*, 1787, 2000.

Frank, L. A., W. R. Paterson, K. L. Ackerson, V. M. Vasyliunas, F. V. Coroniti, and S. J. Bolton, Plasma observations at Io with the Galileo spacecraft, *Science*, *274*, 394, 1996.

Geissler, P. E., A. S. McEwen, W. Ip, M. J. S. Belton, T. V. Johnson, W. H. Smyth, and A. P. Ingersoll, Galileo imaging of atmospheric emissions from Io, *Science*, *285*, 870, 1999.

Goldberg, B. A., Y. Mekler, R. W. Carlson, T. V. Johnson, and D. L. Matson, Io's sodium emission cloud and the Voyager 1 encounter, *Icarus*, *44*, 305, 1980.

Hendrix, A. R., C. A. Barth, and C. W. Hord, Io's patchy $SO_2$ atmosphere as measured by the Galileo ultraviolet spectrometer, *J. Geophys. Res.*, *104*, 11,817, 1999.

Huddleston, D. E., R. J. Strangeway, J. Warnecke, C. T. Russell, and M. G. Kivelson, Ion cyclotron waves in the Io torus: Wave dispersion, free energy analysis, and $SO_2^+$ source rate estimates, *J. Geophys. Res.*, *103*, 19,887, 1998.

Huddleston, D. E., R. J. Strangeway, X. Blanco-Cano, C. T. Russell, M. G. Kivelson, and K. K. Khurana, Mirror-mode structures at the Galileo-Io flyby: Instability criterion and dispersion analysis, *J. Geophys. Res.*, *104*, 17,479, 1999.

Intriligator, D. S., and W. D. Miller, Detection of the Io plasma torus by Pioneer 10, *Geophys. Res. Lett.*, *8*, 409, 1981.

Kivelson, M. G., K. K. Khurana, R. J. Walker, J. Warnecke, C. T. Russell, J. A. Linker, D. J. Southwood, and C. Polanskey, Io's interaction with the plasma torus: Galileo magnetometer report, *Science*, *274*, 396, 1996.

Kumar, S., Sulfur and oxygen escape from Io and a lower limit to atmospheric $SO_2$ at Voyager 1 encounter, *J. Geophys. Res.*, *89*, 7399, 1984.

Lellouch, E., Io's atmosphere: Not yet understood, *Icarus*, *124*, 1, 1996.

Lellouch, E., M. Belton, I. D. Pater, S. Gulkis, and T. Encrenaz, Io's atmosphere from microwave detection of $SO_2$, *Nature*, *346*, 639, 1990.

Lellouch, E., M. Belton, I. D. Pater, G. Paubert, S. Gulkis, and T. Encrenaz, The structure, stability, and global distribution of Io's atmosphere, *Icarus*, *98*, 271, 1992.

Linker, J. A., K. K. Khurana, M. G. Kivelson, and R. J. Walker, MHD simulations of Io's interaction with the plasma torus, *J. Geophys. Res.*, *103*, 19,867, 1998.

Matson, D. L., B. A. Goldberg, T. V. Johnson, and R. W. Carlson, Images of Io's sodium cloud, *Science*, *199*, 531, 1978.

Pilcher, C. B., W. H. Smyth, M. R. Combi, and J. H. Fertel, Io's sodium directional features: Evidence for a magnetospheric-wind-driven gas escape mechanism, *Astrophys. J.*, *287*, 427, 1984.

Russell, C. T., and M. G. Kivelson, Evidence for sulfur dioxide, sulfur monoxide, and hydrogen sulfide in the Io exosphere, *J. Geophys. Res.*, in press, 2001.

Russell, C. T., et al., Mirror-mode structures at the Galileo-Io flyby: Observations, *J. Geophys. Res.*, *104*, 17,471, 1999.

Russell, C. T., M. G. Kivelson, W. S. Kurth, and D. A. Gurnett, Implications of depleted flux tubes in the Jovian magnetosphere, *Geophys. Res. Lett.*, *27*, 3133, 2000.

Russell, C. T., Y. L. Wang, X. Blanco-Cano, and R. J. Strangeway, The Io mass loading disk: Constraints provided by ion cyclotron wave observations, *J. Geophys. Res.*, this issue.

Saur, J., F. M. Neubauer, D. F. Strobel, and M. E. Summers, Three-dimensional plasma simulation of Io's interaction with the Io plasma torus: Asymmetric plasma flow, *J. Geophys. Res.*, *104*, 25,105, 1999.

Scarf, F. L., F. V. Coroniti, D. A. Gurnett, and W. S. Kurth, Pitch angle diffusion by whistler mode waves near the Io plasma torus, *Geophys. Res. Lett.*, *6*, 653, 1979.

Smyth, W. H., Io's sodium cloud: Explanation of the east-west asymmetries, *Astrophys. J.*, *234*, 1148, 1979.

Smyth, W. H., and M. R. Combi, A general model for Io's neutral gas clouds, II, Application to the sodium cloud, *Astrophys. J.*, *328*, 888, 1988.

Smyth, W. H., and M. L. Marconi, An initial look at the iogenic $SO_2^+$ source during the Galileo flyby, *J. Geophys. Res.*, *103*, 9083, 1998.

Summers, M. E., and D. F. Strobel, Photochemistry and vertical transport in Io's atmosphere and ionosphere, *Icarus*, *120*, 290, 1996.

Thorne, R. M., and F. L. Scarf, Voyager 1 evidence for ion-cyclotron instability in the vicinity of the Io plasma torus, *Geophys. Res. Lett.*, *11*, 263, 1984.

Wilson, J. K., and N. M. Schneider, Io's sodium directional feature: Evidence for ionospheric escape, *J. Geophys. Res.*, *104*, 16,567, 1999.

Wong, M. C., and W. H. Smyth, Model calculation for Io's atmosphere at eastern and western elongations, *Icarus*, *146*, 60, 2000.

J. Raeder, C.T. Russell, and Y.L. Wang, Institute of Geophysics and Planetary Physics, University of California, Los Angeles, 405 Hilgard Avenue, Los Angeles, CA 90095-1567, USA. (jraeder@igpp.ucla.edu; ctrussel@igpp.ucla.edu; ylwang@igpp.ucla.edu)

(Received September 26, 2000; revised February 16, 2001; accepted April 19, 2001.)